Check for updates

Global Biogeochemical Cycles

RESEARCH ARTICLE
10.1029/2025GB008576

The Arctic Ocean CO_2 Sink: Trends, Uncertainties, and the Impact of Sea Ice

Victoria R. Dutch[1], Dorothee C. E. Bakker[1], Alizée Roobaert[2], Peter Landschützer[2], Nicholas P. Roden[3], Mario Hoppema[4], and Jan Kaiser[1]

[1]Centre for Ocean & Atmospheric Sciences, School of Environmental Sciences, University of East Anglia, Norwich, UK, [2]Flanders Marine Institute (VLIZ), Ostend, Belgium, [3]Norwegian Institute for Water Research, Bergen, Norway, [4]Alfred Wegener Institute Helmholtz Centre for Polar and Marine Research, Bremerhaven, Germany

Key Points:

- We present a new $p(CO_2)$ product tailored to the Arctic Ocean which provides improved estimates of $p(CO_2)$
- We test 12 different parameterizations for calculating the air-sea CO_2 flux from this new $p(CO_2)$ product
- The parameterization of sea ice adds a considerable amount of uncertainty (up to 25%) to the size of the Arctic Ocean CO_2 sink

Correspondence to:
V. R. Dutch,
v.dutch@uea.ac.uk

Citation:
Dutch, V. R., Bakker, D. C. E., Roobaert, A., Landschützer, P., Roden, N. P., Hoppema, M., & Kaiser, J. (2025). The Arctic Ocean CO_2 sink: Trends, uncertainties, and the impact of sea ice. *Global Biogeochemical Cycles*, *39*, e2025GB008576. https://doi.org/10.1029/2025GB008576

Received 21 MAR 2025
Accepted 9 JUL 2025

Abstract The Arctic Ocean covers 3% of the Earth's surface but is estimated to contribute 5–14% to the global ocean carbon sink. Sparse and unevenly distributed observations complicate our understanding of the size and the controlling mechanisms of this carbon sink. We adopt and advance the two-step neural network approach of Landschützer et al. (2016, https://doi.org/10.1002/2015gb005359; Self Organizing Map—Feed Forward Network) to improve region-specific reconstructions of the surface ocean partial pressure of carbon dioxide ($p(CO_2)$) in the Arctic Ocean and subsequently estimate the air-sea CO_2 flux. Our study shows that biogeochemical properties previously selected as predictor variables for $p(CO_2)$ at the global scale are not well suited to the Arctic Ocean and a sensitivity study reveals large differences in the size of the Arctic Ocean carbon sink depending on the choice of air-sea CO_2 flux parameterization. This is most acute for those relating to sea ice cover, leading to a difference of up to 25% (9.2–13.3 Pg C) in the total size of the Arctic Ocean carbon sink over the 32-year duration of the study.

Plain Language Summary The Arctic Ocean takes up carbon dioxide (CO_2) from the atmosphere, but a limited number of observations of the amount of CO_2 in the Arctic Ocean prevent us from making a precise estimate of the size of this carbon sink. Here, we use a machine learning method to interpolate observations of surface ocean CO_2 in time and space in regions lacking in data in order to quantify the size of the Arctic Ocean carbon sink. Uncertainty in the role of sea ice cover when calculating CO_2 flux leads to differences in the size of the Arctic Ocean carbon sink, with an up to 25% difference in the size of the Arctic Ocean carbon sink between different versions of the flux calculation over the 32-year study period.

1. Introduction

Over a quarter of anthropogenic carbon dioxide (CO_2) emissions since pre-industrial times are stored in the oceans (Gruber et al., 2023), acting as a buffer against rising atmospheric CO_2 concentrations and subsequent climate change. The Arctic Ocean region plays a disproportionately large role in the ocean carbon sink, contributing 5–14% toward the global ocean CO_2 sink when covering only 3% of the Earth's surface (Bates & Mathis, 2009). The Arctic is at the forefront of global climate change, with rapid sea-ice decline expected to have a subsequent impact on the biogeochemistry of the Arctic Ocean (Lannuzel et al., 2020). Several different processes in the Arctic Ocean act to drive carbon uptake from the atmosphere and its sequestration into the deep ocean, however, these are not well-constrained. The interplay of these processes and how they have been and continue to be affected by climate change limit our understanding of the Arctic Ocean carbon sink (Juranek, 2022; Tremblay et al., 2015).

Ocean carbon uptake is driven by the difference in partial pressure of CO_2 ($p(CO_2)$) between the ocean (locally variable) and the atmosphere (more globally homogenous). Measurements of sea surface $p(CO_2)$ in remote, often frozen, regions such as the Arctic are logistically complex. As a result, data across the Arctic are sparse (Figure A1), with no data available for sizable parts of the region - particularly in perennially ice covered areas. Data availability is also highly seasonal, with a far greater number of measurements in the summer months (June to September, JJAS), particularly at higher latitudes (Figure A1). Issues surrounding the low abundance of $p(CO_2)$ observations are unlikely to be resolved in the near future due to financial and geographical constraints and reduced observation frequency (Rustogi et al., 2023), with the sparsity of observations having increased from 2018 onwards (Dong, Bakker, & Landschützer, 2024). This impairs our ability to understand and predict trends and changes in the Arctic Ocean carbon sink, particularly at seasonal timescales (Rustogi et al., 2023). Seasonal

© 2025. The Author(s).
This is an open access article under the terms of the Creative Commons Attribution License, which permits use, distribution and reproduction in any medium, provided the original work is properly cited.

biases in measurements of other variables used to deepen our knowledge of the ocean carbon sink, particularly those relating to sea ice (Gerland et al., 2019), also limit our understanding. Although biogeochemical ocean models and Earth system models provide a lens into a changing Arctic, this can only go so far as the representation of biogeochemical processes at play in the Arctic is often poor (Popova et al., 2012). Differences persist between estimates of the magnitude of the ocean carbon sink from observation-based products and biogeochemical models, with this discrepancy exacerbated at regional scales - particularly for under-sampled regions such as the Arctic where such differences are of the order of magnitude of 20 Tg of carbon per year (Friedlingstein et al., 2022; Yasunaka et al., 2023).

Improving the coverage of surface ocean $p(CO_2)$ can help us to improve our understanding of the Arctic Ocean carbon sink and its spatio-temporal variability. Globally, numerous approaches have been taken to interpolate across limited observations of surface ocean $p(CO_2)$, from linear regressions (Iida et al., 2021; Lefèvre & Taylor, 2002) to complex machine learning approaches (see Rödenbeck et al., 2015; Gregor et al., 2019; Fay et al., 2021, for an overview). One such machine learning approach is the Self Organising Map - Feed Forward Network (SOM-FFN) approach, first developed by Landschützer et al. (2013) in a study of the North Atlantic Ocean and subsequently applied at multiple spatial resolutions at local, regional and global scales (e.g., Duke et al., 2023; Laruelle et al., 2017; Roobaert et al., 2024; Landschützer et al., 2020, among others). However, the accuracy of such (typically global) $p(CO_2)$ products in polar regions, where $p(CO_2)$ measurements are sparse, remains poor (Zhong et al., 2024). Estimates of high-latitude ocean CO_2 uptake from existing $p(CO_2)$ products not only differ from each other (Landschützer et al., 2020), but also from ocean biogeochemical model simulations (Hauck et al., 2023). Differences between these $p(CO_2)$ products are particularly pronounced in terms of seasonal variability (Rustogi et al., 2023), and half of all $p(CO_2)$ products included in the Arctic chapter of the most recent RECCAP (REgional Carbon Cycle Assessment and Processes) report do not cover the full Arctic region including the sea-ice zones (Yasunaka et al., 2023). Such products are not typically derived with the Arctic Ocean as their focus (with that of Yasunaka et al. (2018) as the key exception), and therefore the representation of and inferences made about processes unique to the Arctic Ocean are at best incidental.

We present a new $p(CO_2)$ product for the Arctic Ocean using only data from this region in order to constrain the size of the Arctic Ocean carbon sink. In particular, we examine the role of sea ice in introducing uncertainty in the Arctic Ocean carbon sink, and test a number of approaches to the parameterisation of ocean-atmosphere CO_2 fluxes in the Arctic sea ice zone.

2. Data and Methods

We define the Northern polar ocean region in our study as the domain northwards of 55°N, excluding the Baltic Sea (53–66°N, 10–30°E), and refer to this domain as the Arctic Ocean. We examine the period from January 1991 to December 2022, producing monthly estimates as well as an overall period averaged $p(CO_2)$ climatology at $1° \times 1°$ resolution. We subsequently calculate air-sea CO_2 fluxes from these $p(CO_2)$ values and perform a sensitivity analysis on these fluxes and then produce monthly maps and a time averaged climatology at the same spatial resolution. Both $p(CO_2)$ and CO_2 flux products are available at: https://doi.org/10.5281/zenodo.15056124.

In this section, we first describe the neural network method used to generate the $p(CO_2)$ product. Secondly, we lay out how the $p(CO_2)$ product will be evaluated. We then perform a sensitivity analysis on the calculated CO_2 flux, before finishing with the approach for comparing the CO_2 flux estimates.

2.1. Neural Network Configuration

We use the two-step SOM-FFN neural network approach of Landschützer et al. (2013) to reconstruct monthly maps of $p(CO_2)$ in the Arctic Ocean. First, a Self-Organizing Map (SOM) neural network is used to divide the study area into biogeochemical provinces that have similar biogeochemical properties. For each of these provinces, a Feed Forward Neural network (FFN) is then used to compute non-linear relationships between direct observations of $p(CO_2)$ from the SOCATv2022 gridded product (Surface Ocean CO_2 ATlas; Bakker et al., 2022) and other selected biogeochemical properties, which are then used to interpolate $p(CO_2)$ values for grid cells where no $p(CO_2)$ observations are present. The final product is in the form of monthly $p(CO_2)$ maps at a $1° \times 1°$ resolution for the 1991–2022 period. Seasonal gaps exist in the final product when observations of biogeochemical predictor variables are not available; this occurs exclusively at higher latitudes, predominantly in the Siberian Sea.

Table 1
Description of Neural Network Driving Data and Data Sets Used for the Subsequent Calculation of Air-Sea CO_2 Fluxes

Environmental driver	Neural network step: SOM	Neural network step: FFN	Resolution	Manipulation	Reference
$p(CO_2)$		X	1° × 1°	Conversion from $f(CO_2)$	SOCATv2022; Bakker et al. (2022)
SST[a]	X	X, anomaly	0.25° × 0.25°	Calculation of anomaly as additional FFN driver	Reynolds et al. (2007)
SSS[a]	X	X, anomaly	0.25° × 0.25°	Calculation of anomaly as additional FFN driver	Good et al. (2013)
MLD	X		0.5° × 0.5°	Log-Transformation	MIMOC; Schmidtko et al. (2013)
Wind speed at 10 m above sea level[a]		X	0.25° × 0.25°		ERA5; Hersbach et al. (2019)
Sea Ice Cover[a]		Sea Ice Change	0.25° × 0.25°	Calculation of Sea ice change and Location of Sea ice cover province	HADISST; Rayner et al. (2003)
Bathymetry		X	2 min (0.03° × 0.03°)		ETOPO v2; National Geophysical Data Center (2006)
Atmospheric CO_2 partial pressure[a]		X, anomaly		Calculation of anomaly as additional FFN driver	Dlugokencky et al. (2019)

[a]Also used for the CO_2 flux calculations.

2.1.1. Self Organizing Map

We configure the SOM neural network following Landschützer et al. (2013), except for the modifications described below. Previous studies (Landschützer et al., 2020) have found an improvement in the estimation of Arctic surface ocean $p(CO_2)$ when only using data from within the Arctic region. We extend this idea by only using data from our definition of the Arctic and allowing for spatial and temporal variability in the relationships between $p(CO_2)$ and environmental predictor variables through the use of multiple biogeochemical provinces in the SOM, rather than taking the Landschützer et al. (2020) approach whereby the Arctic is contained within a single time-invariant province. Deriving biogeochemical provinces for each time step, rather than the use of a static, time-invariant province configuration allows the impact of freeze-up, ice melt, spring blooms, and other important seasonal processes to be captured.

For both the SOM and the FFN, we use a set of input parameters taken from large gridded data sets to drive the machine learning model. These data products, chiefly from either remote sensing or atmospheric reanalysis, are described in detail in Table 1. We source the following variables to act as input parameters into either one (or both) of the two steps of the neural network; sea surface temperature (SST), sea surface salinity (SSS), mixed layer depth (MLD), wind speed, bathymetry, sea ice cover, sea ice change (derived as sea ice cover minus the sea ice cover of the previous month), and atmospheric mole fraction of CO_2. For the MLD, we use a climatology (MIMOC; Schmidtko et al., 2013) and log transform these data prior to their inclusion in the neural network, following Landschützer et al. (2013). We also included anomalies of SST, SSS and atmospheric CO_2, where the long term trend was removed from each of these data sets to look at the relative impact of short-term variability. All input parameters were rescaled to monthly 1° × 1° resolution prior to our analysis. We test 16 input parameter combinations for the SOM to construct a set of biogeochemical provinces: SST, SSS, MLD, wind speed, bathymetry, and sea ice cover. All tests include SST, SSS and MLD. Similar to the findings of Duke et al. (2023) for the Alaskan Pacific (a region which overlaps with our domain), we find the best SOM predictor variables to be SST, SSS, and MLD.

The $p(CO_2)$ climatology of Takahashi et al. (2009), previously used in similar studies (Landschützer et al., 2013, 2014, 2020), is inappropriate in our case due to zero data coverage above 80°N and very limited data availability throughout the rest of the study area, and low spatial resolution (5° × 5°) relative to the size of our domain. We also exclude chlorophyll *a* concentration, used in most similar products, due to a lack of satellite-derived optical data availability during polar night.

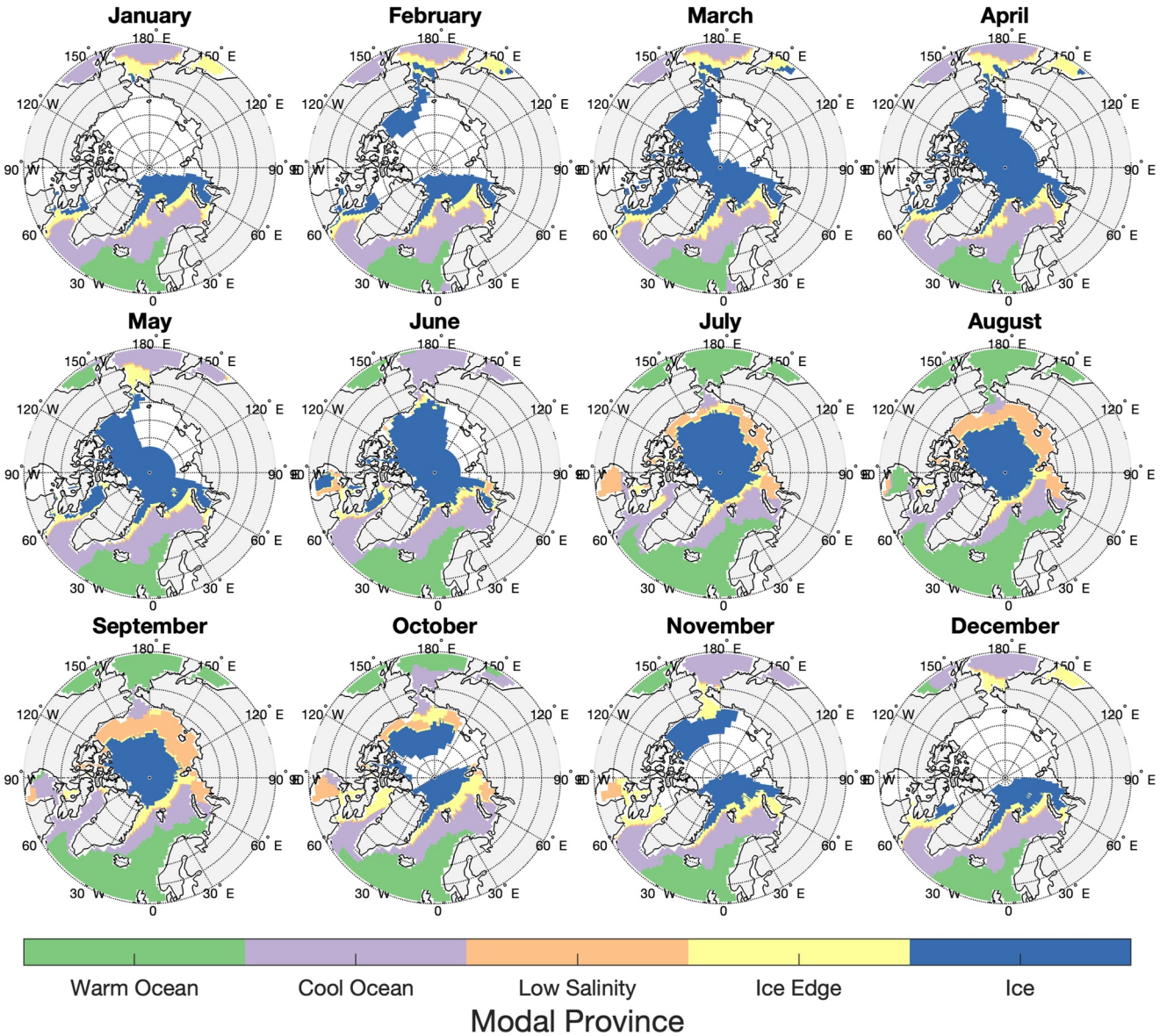

Figure 1. The most common biogeochemical province for each grid cell derived from the Self Organizing Map. Note that these biogeochemical provinces are derived for each month, and this figure shows an aggregate for each calendar month over the entire 32-year period.

The SOM initially produces four biogeochemical provinces; tests using additional SOM provinces led to network instability during the FFN stage as the additional biogeochemical province had less than the minimum number of grid cells required for validation. For each time step, we also separate all grid cells with greater than 85 % ice cover into an additional (fifth) province. This is due to known issues with satellite retrievals of biophysicochemical properties under sea ice (e.g., Smith et al., 2019), and as Yasunaka et al. (2018) determined that separation of ice-covered and ice-free regions gives an improved estimate of Arctic Ocean carbon flux.

The most common biogeochemical provinces for each grid cell for each calendar month of the 32 years analysis period are presented in Figure 1, with each province described in Table 2. Biogeochemical provinces cannot be derived for all grid cells and time steps - the High Arctic, particularly off the coast of Siberia, is missing data for a significant part of the year. This is not unique to our product, and has been found for the Arctic region of global products by other studies (Ritschel et al., 2024). Not all biogeochemical provinces persist for all months of the year, with the low salinity province only present from June to November.

Table 2
Representation of the 5 Monthly Biogeochemical Provinces and Mean $\bar{p}(CO_2)$ Differences Between the SOM-FFN Product and SOCAT v2023

Biogeochemical province description	Proportion of grid cells (%)	n(SOM-FFN)	n(SOCAT)	R^2(SOCAT vs. SOM-FFN)	$\bar{p}(CO_2$, SOM-FFN) − $\bar{p}(CO_2$, SOCAT) (µatm)
Warm Ocean	9.06	282 965	22 449	0.67	1.4
Cool Ocean	12.0	388 340	11 583	0.73	0.9
Low Salinity	3.05	102 624	3 115	0.49	3.5
Ice Edge	5.25	179 696	1 382	0.54	2.5
>85% sea ice cover	34.3	1 137 449	3 126	0.60	7.3

Note. The proportion of the domain represented by each of the 5 biogeochemical provinces (quantified as the percentage of grid cells contained in each province, not the percentage of the domain area) do not add up to 100% as biogeochemical provinces could not be derived for all grid cells and monthly time steps.

2.1.2. Feed Forward Network

After the biogeochemical provinces have been derived, a FFN is used to determine non-linear relationships between $p(CO_2)$ (taken from the SOCATv2022 gridded product) and other biogeochemical properties (or proxies) that are linked to $p(CO_2)$ variability for each province. We test 32 different combinations of proxies into the FFN after those used by Landschützer et al. (2020) and Roobaert et al. (2024). All tests included SST, SSS (both values and anomalies, with anomalies calculated as the difference between the value for a grid cell for a given month and the mean value for that grid cell for that month of the year) and atmospheric $p(CO_2)$, alongside a combination of wind speed, bathymetry, sea ice cover, sea ice change and atmospheric CO_2 anomaly (including one test where none of these additional variables were included). Sea ice change was calculated as the sea ice cover minus the sea ice cover of the preceding month.

Resulting $p(CO_2)$ values produced using the 32 input parameter combinations for the FFN varied less than for the different biogeochemical province combinations, suggesting that the derivation of biogeochemical provinces is more important in determining $p(CO_2)$ values. Several sets of FFN input parameters performed well (as quantified by high R^2, lower root mean square error (RMSE) and mean difference values when compared to the SOCAT v2023 gridded product) for the different seasons, regions and latitude bands. Although mean $p(CO_2)$ values for the different FFN networks varied considerably (range of 35 µatm), mean differences from SOCAT were always within the uncertainty of Flag E SOCAT data (<10 µatm), and typically within the uncertainty of the SOCAT gridded data product used herein (<5 µatm).

Across different spatio-temporal divisions of the model domain, the combination of atmospheric CO_2 anomaly, bathymetry and sea ice change (alongside the variables SST, SSS and atmospheric $p(CO_2)$ included in all tests) consistently performed highly and thus was chosen as the final set of FFN inputs. We then reran this configuration of the FFN to get a total of 10 repeat runs withholding a different subset of data for internal validation each time (i.e., a Monte Carlo type approach), and use the ensemble mean as our final $p(CO_2)$ product, as the use of an ensemble mean has been shown to improve the robustness and reliability of this approach (Duke et al., 2023). We also produce a $p(CO_2)$ climatology, where we detrend the increase in $p(CO_2)$ over the time period covered by our product by removing the increasing 12 months running mean atmospheric $p(CO_2)$ trend from our time series, and then derive a climatological mean $p(CO_2)$ map for each month of the calendar year.

2.2. Evaluation of $p(CO_2)$ Product

We evaluate our reconstructed $p(CO_2)$ product against the limited available data in the Arctic domain that were not initially used to train the neural network. We chiefly compare to $p(CO_2)$ measurements from the SOCATv2023 gridded product (Surface Ocean CO_2 ATlas; Bakker et al., 2016, 2023, with v2023 being the subsequent edition to that used to develop the SOM-FFN product), and to independent time series data not included in the SOCAT v2022 gridded product (Bakker et al., 2022) and thus not used in the reconstruction of our SOM-FFN $p(CO_2)$ product. We converted SOCAT observations of fugacity of CO_2 ($f(CO_2)$) to $p(CO_2)$ as given in Körtzinger (1999). Independent time series data was either that contained within the SOCAT database but excluded from the gridded product (termed Flag E SOCAT data) or preliminary data from the year-long MOSAiC campaign (Multidisciplinary drifting Observatory for the Study of Arctic Climate; Shupe et al., 2022) - also with

the same uncertainty as the flag E SOCAT data. Locations of all independent data sets used for evaluation are shown in Figure A2. In order to expand our evaluation data set, we also calculate $p(CO_2)$ values from observations of dissolved inorganic carbon (DIC) concentrations and total alkalinity (TA), sourced from GLODAPv2 (GLobal interior Ocean biogeochemical DAta Product; Olsen et al., 2016; Lauvset et al., 2016, 2024), using CO2SYS (Lewis & Wallace, 1998) for Matlab v3.2.1 (Sharp et al., 2023). We use the K_1 and K_2 coefficients of Millero et al. (2002), the $K(H_2SO_4)$ dissociation constant from Dickson (1990), the K(HF) dissociation constant of Perez and Fraga (1987) and the borate-to-salinity ratio of Lee et al. (2010). This allows us to compare to surface ocean (<10 m) measurements of carbonate chemistry variables from GLODAPv2, and from bottle samples such as those from the MOSAiC campaign (Fong et al., 2024; Torres-Valdés et al., 2024a, 2024b; Ulfsbo et al., 2023). For each CTD cast, we take the mean values of DIC concentration, TA and nutrient concentrations for all samples in the upper 10 m of the water column, and from these calculate $p(CO_2)$ in CO2SYS as outlined above. For the MOSAiC underway data, we include all $p(CO_2)$ measurements with a quality flag of 1 from the quality control software QuinCe (Jones & Henriksen, 2018; Steinhoff et al., 2019), indicative of good quality data following the SOCAT quality control cookbook (Gkritzalis et al., 2024).

We also compare our $p(CO_2)$ product to other $p(CO_2)$ products with Arctic coverage, but that largely were not specifically designed for the Arctic region, in order to assess the improvement made by our region-specific changes.

Following Landschützer et al. (2014), we consider uncertainties in our $p(CO_2)$ product to be a result of errors in either the $p(CO_2)$ measurement, the [re]gridding of the measurements, or from the reconstruction of the $p(CO_2)$ using the SOM-FFN (derived from a comparison to the SOCATv2023 database). These errors are then propagated in quadrature to give the overall error of the $p(CO_2)$ product (Roobaert et al., 2019):

$$\theta(p(CO_2)) = \sqrt{\left(\frac{\theta_{obs}}{\sqrt{N}}\right)^2 + \left(\frac{\theta_{grid}}{\sqrt{N}}\right)^2 + \left(\frac{\theta_{map}}{\sqrt{N_{eff}}}\right)^2} \quad (1)$$

where N is the number of grid cells containing a $p(CO_2)$ value in the SOCAT gridded product. For the mapping term, an effective N value (N_{eff}) is used, which is adjusted to account for spatial autocorrelation as given in Landschützer et al. (2018).

2.3. Air-sea CO_2 Exchange

From the final $p(CO_2)$ product, we then determine air-sea CO_2 exchange to assess the size of the Arctic Ocean carbon sink and its spatio-temporal variability.

In order to examine the uncertainty surrounding estimates of Arctic Ocean air-sea CO_2 fluxes, we perform a sensitivity analysis and test a number of different parameterizations involved in the CO_2 flux calculation. First, we examine the impact of the chosen gas exchange transfer coefficient k, following both the formulas of Wanninkhof (2014):

$$k/(\mathrm{cm\,h^{-1}}) = 0.251 <U_{10}^2>/(\mathrm{m^2\,s^{-2}})(Sc/660)^{-0.5} \quad (2)$$

and Nightingale et al. (2000):

$$k/(\mathrm{cm\,h^{-1}}) = [0.333 <U_{10}>/(\mathrm{m\,s^{-1}}) + 0.222 <U_{10}^2>/(\mathrm{m^2\,s^{-2}})](Sc/600)^{-0.5} \quad (3)$$

where $<U_{10}>$ is the monthly mean wind speed at 10 m above sea level and $<U_{10}^2>$ is its second moment. Sc represents the Schmidt number (Wanninkhof, 2014). We also test the impact of the lower value for the gas transfer coefficient in Equation 2 suggested for sea ice areas by Prytherch and Yelland (2021) (0.179) in all grid cells with a sea ice fraction greater than 0.1. When referring to the Prytherch parameterization, fluxes for grid cells with a sea ice fraction of 0.1 or less continue to be calculated using Wanninkhof (2014) (Equation 2).

For sea-ice covered grid cells, we scale the fluxes to the sea ice extent (f_{ice}; value between 0 and 1). We test both the typically used linear (Butterworth & Miller, 2016) sea-ice scaling parameterization:

$$F = \left(1 - f_{ice}\right) kK_0 \Delta p(CO_2) \quad (4)$$

and the non-linear parameterization of Loose et al. (2009):

$$F = \left(1 - f_{ice}\right)^{0.4} kK_0 \Delta p(CO_2) \quad (5)$$

In both cases, K_0 is the solubility coefficient of CO_2 in seawater in mol m^{-3} atm^{-1}, which depends on SST and SSS (Weiss, 1974), and $\Delta p(CO_2)$ is the CO_2 partial pressure difference between surface ocean and atmosphere in μatm (with the atmospheric mole fraction of CO_2 converted to μatm as per Appendix 3 of Landschützer et al. (2013)). A positive flux indicates a flux of CO_2 from ocean to atmosphere (i.e., the Arctic Ocean being a CO_2 source). The non-linear parameterization has been used in the Arctic assessment of Yasunaka et al. (2018), but not for Arctic regions of global $p(CO_2)$ products. We also test setting the maximum sea ice cover fraction to 0.9 to account for uncertainties of up to 10% in the amount of ephemeral open water unaccounted for in satellite retrievals of sea ice cover (Loose et al., 2014; Takahashi et al., 2009), and term this the Max 90% Ice parameterization.

We calculate cumulative estimates of the Arctic Ocean carbon sink for each combination of these different parameterizations (12 in total). These CO_2 fluxes are then compared to each other and to the ensemble mean Arctic Ocean carbon sink presented in RECCAP2 (Yasunaka et al., 2023), noting that RECCAP2 uses a far smaller spatial definition of the Arctic Ocean which does not include the North Atlantic region.

3. Results and Discussion

3.1. $p(CO_2)$

3.1.1. Characteristics of the New $p(CO_2)$ Product

Detrended annual mean surface ocean $p(CO_2)$ for 1991 to 2022 are shown in Figure 2. Surface ocean $p(CO_2)$ from our new product has a spatio-temporal averaged median value of 308.3 μatm, a mean value of 311.2 µatm and a standard deviation of 48.5 µatm. Note that these values only include grid cells with data, and so are likely to be biased away from the Laptev and East Siberian Sea region where year-round $p(CO_2)$ values are not available. In order to look at spatial differences in $p(CO_2)$ across the Arctic domain and how well these are reproduced by our SOM-FFN product, we split our domain into three latitude bands (Table 3). As a greater number of $p(CO_2)$ products are available for the Sub-Arctic, we considered SOM-FFN performance here to be less important than performance in the High Arctic when choosing our best neural network configuration. This is, however, complicated by considerably lower data availability further north (see n values in Table 3), due both to logistical constraints of northern sampling and to the lower relative surface area of grid cells at higher latitude.

Simulated $p(CO_2)$ from the SOM-FFN product is well matched to observed values, with a mean bias from SOCATv2023 of +1.9 µatm across the entire spatio-temporal coverage of the SOM-FFN product. Evaluating our SOM-FFN product against SOCATv2023 gives an RMSE of 29.1 µatm, significantly greater than the uncertainty given for SOCAT observations (2–5 µatm), but comparable to global RMSE estimates for similar products (Gloege et al., 2022). When only looking at co-located data points, the SOM-FFN product and SOCATv2023 are shown to have a very similar data distribution and median $p(CO_2)$ values (Figure 3b). However, when extrapolating outside of this area, the SOM-FFN product suggests lower $p(CO_2)$ values than seen in the SOCAT gridded product (Figure 3a).

Monthly average values for the three latitude bands are all biased high in the SOM-FFN relative to SOCAT observations (Table 3), with differences from SOCAT greatest in the High Arctic. Table 2 shows the five different biogeochemical provinces to have noticeable variation in their mean differences from SOCAT, with poorer emulation of SOCAT observations found in ice-affected provinces than in the open ocean. Median differences from SOCAT for each biogeochemical province are all slightly higher than mean values, but the relative performance of each province stays the same. We also considered evaluating our simulated $p(CO_2)$ values by RECCAP biome, after Yasunaka et al. (2023). However, data availability varies greatly between RECCAP biomes, with one RECCAP biome (Baffin Bay) having only six SOCAT observations and six out of ten RECCAP biomes having no available $p(CO_2)$ measurements during spring or winter.

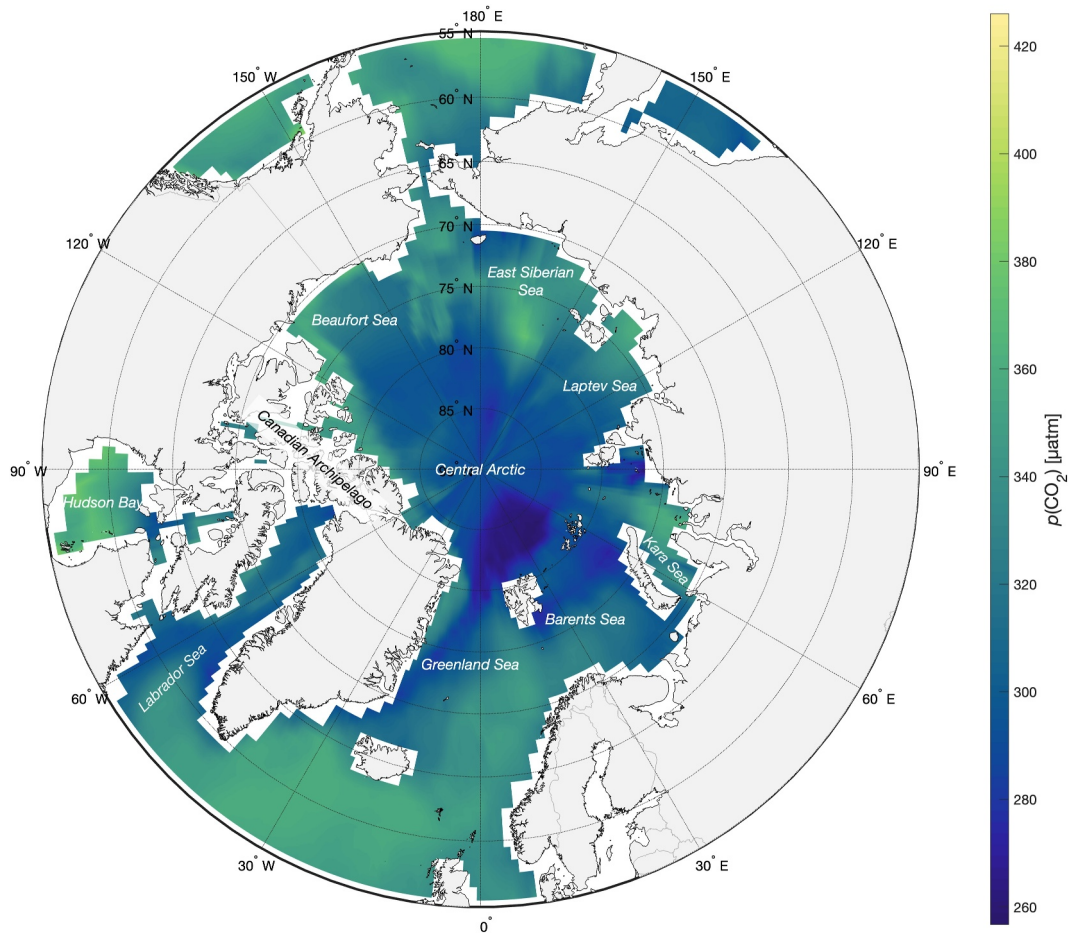

Figure 2. Climatological detrended annual mean surface ocean $p(CO_2)$ across the Arctic Ocean domain (north of 55°N for the period January 1991–December 2022), derived from the Self Organising Map–Feed Forward Network.

We then compare both the SOM-FFN $p(CO_2)$ product and the SOCAT gridded $p(CO_2)$ to $p(CO_2)$ derived from measurements of TA and DIC concentration from the GLODAP database, as shown in Figure 3c. For this, we take all measurements above a depth of 10 m, derive $p(CO_2)$ as described above, and then match these derived $p(CO_2)$ values to their corresponding grid cells in the $p(CO_2)$ and SOCAT gridded products. Generally speaking, there is good agreement between the $p(CO_2)$ product and GLODAP, with a mean difference (SOM-FFN - GLODAP) of 6.9 µatm, well within the 12 µatm uncertainty given for $p(CO_2)$ derived from GLODAP by Gregor et al. (2019). Median $p(CO_2)$ values for all three data sets (subset to where GLODAP data are available) are all within 6 μatm, with the smallest difference in medians between GLODAP and our $p(CO_2)$ product. Mean differences between our $p(CO_2)$ product and the GLODAP data vary latitudinally, with the smallest differences in the High Arctic (−2.2 µatm) and the greatest differences in the Low Arctic (8.8 µatm). GLODAP observations, being more representative of small scale processes and sub-grid cell heterogeneity than monthly 1° × 1° values, give a much broader distribution than the SOCAT gridded product or the SOM-FFN data product, leading to a very high standard deviation (112 µatm) and RMSE (113 µatm).

We next compare the relative similarity to the SOCATv2023 gridded product for our Arctic SOM-FFN and three other leading $p(CO_2)$ products with at least partial coverage of our Arctic domain; Jersild et al. (2017), Roobaert et al. (2024), and Yasunaka et al. (2018). We re-grid the Roobaert et al. (2024) product to the 1° × 1° spatial resolution used by the other products. Note that the temporal and spatial coverage of all four products is slightly different, with no data outside of the coastal zone or after 2020 in the Roobaert et al. (2024) product, no data before 1997 or after 2017 in Yasunaka et al. (2018), and no data after 2021 in the Jersild et al. (2017) product.

Table 3
Mean of $p(CO_2)$ Product by Latitude Band for 1991 to 2022 and Comparison With SOCAT v2023 Data

Latitude	n(SOM-FFN)	n(SOCAT)	R^2(SOCAT vs. SOM-FFN)	$\bar{p}(CO_2$, SOM-FFN) [µatm]	$\bar{p}(CO_2$, SOM-FFN) − $\bar{p}(CO_2$, SOCAT) [µatm]	σ(SOM-FFN-SOCAT) [µatm]
Sub-Arctic (55.0–66.0°N)	436 356	35 572	0.67	339	1.9	27.0
Low Arctic (66.0–78.0°N)	628 246	14 362	0.58	321	1.0	32.1
High Arctic (>78.0°N)	1 026 472	3 843	0.64	293	5.0	30.2

Note. n denotes the number of monthly grid cells containing $p(CO_2)$ values.

Mean and median differences from SOCAT are positive for our product but negative for the others (Table 4). The spread of mean residuals when compared to SOCATv2023 is also less pronounced for our product than for these other products. The SOCAT RMSE for the Jersild et al. (2017) and Yasunaka et al. (2018) products are greater than that for our $p(CO_2)$ product, while the RMSE of the Roobaert et al. (2024) product is similar to ours. We note, however, the difference in coverage of the Roobaert et al. (2024) product in comparison to our own, and so this calculated RMSE value includes a smaller number of $p(CO_2)$ values and does not include the ice-covered Central Arctic region where uncertainty tends to be greater.

3.1.2. Validation With Independent Timeseries Data

Two Icelandic time series are included within our study area, with measurements of surface ocean carbonate variables taken three or four times a year. We compare these time series of surface ocean $p(CO_2)$ for the Iceland

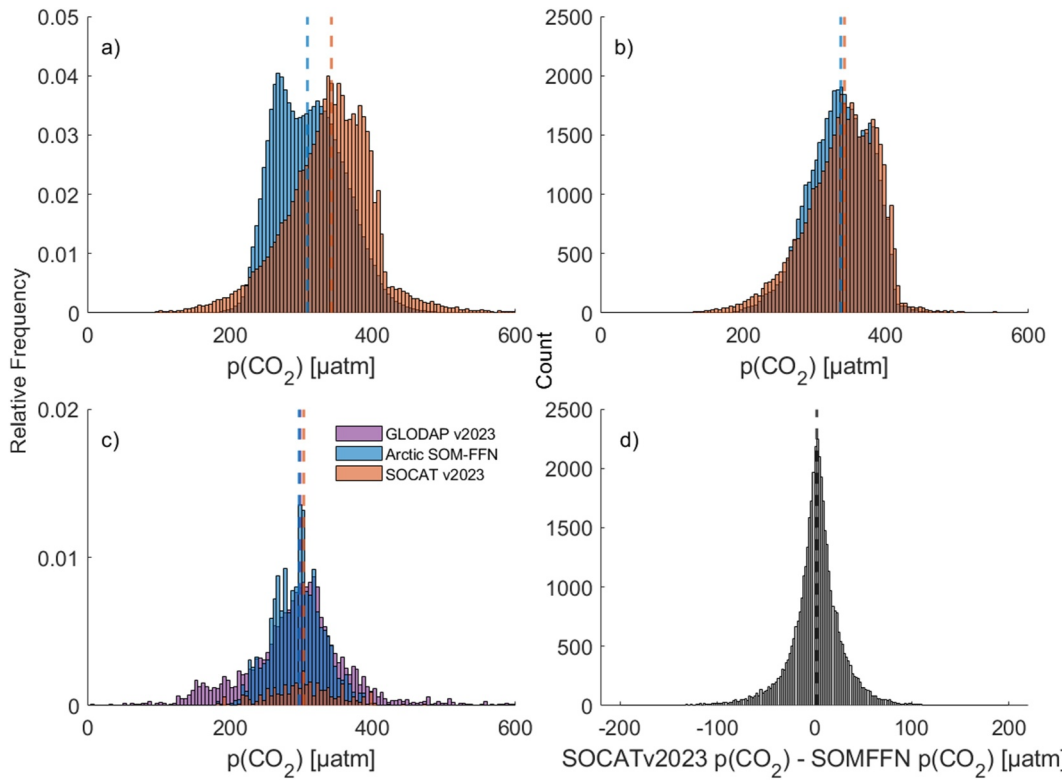

Figure 3. Distribution of monthly $p(CO_2)$ values from both the Self Organising Map-Feed Forward Network (SOM-FFN) product and SOCATv2023 for 1991 to 2022 for (a) the entire SOM-FFN domain and (b) only time steps and grid cells where both SOCAT and SOM-FFN data are available. (c) Distribution of $p(CO_2)$ values from GLODAP, SOCAT and the SOM-FFN product, only for grid cells where GLODAP data are available. (d) Difference between SOCATv2023 and SOM-FFN $p(CO_2)$ values where both are available. In all cases, vertical dashed lines represent the median value and colors for each dataset are the same on all 4 panels. Note that the y-axes for (a, c) are given on a relative abundance scale, whereas (b, d) use the same scale denoting the absolute number of $p(CO_2)$ values.

Table 4
Comparison of the New $p(CO_2)$ Product Against Others With at Least Partial Arctic Coverage

$p(CO_2)$ product	Area covered	Dates covered	Mean Dif. [µatm] (Product−SOCAT)	RMSE [µatm] (Product−SOCAT)
Arctic SOM-FFN	55°–90°N	1991–2022	1.9	29
Jersild et al. (2017)	Global	1983–2020	−1.6	36
Roobaert et al. (2024)	Global Coastal Ocean	1983–2021	−3.8	28
Yasunaka et al. (2018)	RECCAP Arctic Basin	1997–2017	−1.97	66

Note. Values given in the final two columns compare each product to SOCAT within the spatio-temporal domain of our new SOM-FFN product (as given in the first row). Additionally, the Roobaert product does not produce $p(CO_2)$ estimates for most of the Central Arctic.

(68.0°N, 12.7°W) and Irminger Sea (64.3°N, 28.0°W) stations to the SOM-FFN product in Figure 4. Prior to 2014, we use discrete $p(CO_2)$ measurements from these stations (Olafsson et al., 2010). From 2014 onwards however, $p(CO_2)$ was no longer measured for these time series and so we derived $p(CO_2)$ from DIC concentration and TA. Mean differences between direct observations of $p(CO_2)$ and reconstructed $p(CO_2)$ from the SOM-FFN product are less than 5 µatm for the Irminger Sea station (Figure 4b), and 13 µatm for the Iceland Sea station (Figure 4a). Differences between time series data and the $p(CO_2)$ product are higher for the section of the time series where the $p(CO_2)$ is derived from DIC concentration and TA, with a positive bias found when using both the Millero et al. (2002, as shown in Figure 4) or Sulpis et al. (2020) dissociation constants. The seasonality of the SOM-FFN product is well matched to the observations at both stations, with the largest difference between the observations and the SOM-FFN product typically occurring in May.

SOCAT data with a quality flag E, representative of an uncertainty of up to 10 µatm is not included in the SOCATv2022 and SOCATv2023 gridded products and is here used as independent data to compare to individual grid cells of the SOM-FFN product. Within our Arctic domain, we find three different flag E data sets: one stationary buoy; Station M (located at 65.8°N, 2.18°E; Skjelvan & Lauvset, 2018), one drifting buoy; CARIOCA (moving around the Greenland Sea; Merlivat, 2011; Hood et al., 1999), and one vessel; the Lysbris Seaways (regularly traveling between Norway, Denmark, and the United Kingdom; split into two different records (A and B) to remove one and a half years of highly intermittent data; Macovei, Voynova, et al., 2021; Macovei, Petersen, et al., 2021). For each record, every measurement was binned into the same 1° × 1° × 1 month bins used by the

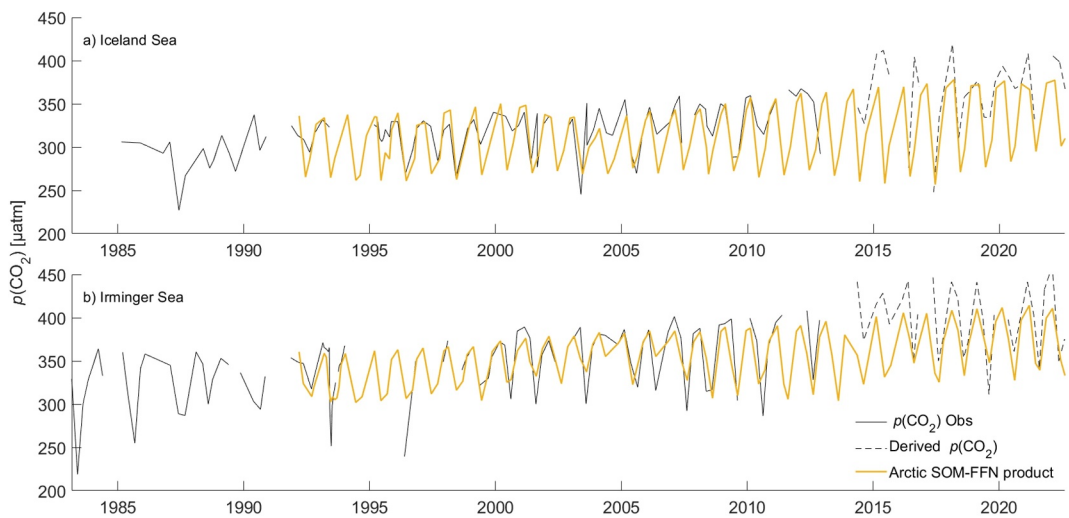

Figure 4. Timeseries of $p(CO_2)$ for the (a) Iceland Sea and (b) Irminger Sea stations, both from observations (black; Olafsson et al., 2010) and from the Self Organising Map–Feed Forward Network product (yellow). The locations of both stations are given in Figure A2.

Table 5
Summary of Each of the $p(CO_2)$ Comparisons

Timeseries	Dates	Location	Mean Dif. [µatm] (Timeseries - SOMFFN)	Std. Dev. [µatm]	RMSE [µatm]
Iceland[a]	February 1992–November 2012	Iceland Sea	13	26	29
Irminger[a]	Febuary 1992–November 2012	Irminger Sea	4.2	26	26
Station M	May 2016–June 2017	Iceland Sea	−11	16	19
CARIOCA	August 1996–April 1997	Greenland Sea	9.9	23	23
Lybris Seaways (A)	September 2013–January 2019	Norwegian and North Seas	26	30	39
Lybris Seaways (B)	September 2021–August 2022	Norwegian and North Seas	−12	38	39
MOSAiC[a]	September 2019–October 2020	Central Arctic Ocean	6.6	24	23

[a]Denotes timeseries with both measured and derived $p(CO_2)$, although only the directly measured values are used for the comparison in this table. The location and tracks for each timeseries are shown in Figure A2.

SOM-FFN. These binned observational values were then compared to the weighted mean of the SOM-FFN $p(CO_2)$ values from the latitude/longitude bins visited by the observing platform during each given month (Table 5).

It should be cautioned that measurements from a single cruise or buoy track, as evaluated in this section, may not be representative of the monthly mean grid cell $p(CO_2)$ value - particularly in regions with large day-to-day variability or sub-grid cell spatial heterogeneities (Yasunaka et al., 2016). We also note that cruises likely travel between several grid cells within the course of a month, and although a weighted average of the time spent in each grid cell is used, this may still impact the fit between observed data and the $p(CO_2)$ product, particularly for regions with high levels of spatial heterogeneity. Additionally, as observations from these data sets are of a much higher temporal resolution (sub-daily) than the monthly SOM-FFN product, these will inherently be noisier.

Mean differences between our $p(CO_2)$ product and the quality flag E data sets, except Station M, are positive (Table 5). RMSEs between the flag E data sets and the SOM-FFN product are within the approximate range of global ocean RMSE estimates for both this and other $p(CO_2)$ products, with those for Station M and CARIOCA lower than found for the $p(CO_2)$ product as a whole. Comparison with these independent data sets again shows that the amplitude of the seasonal cycle of $p(CO_2)$ is not captured in the SOM-FFN product, with the largest negative differences (i.e., SOM-FFN $p(CO_2)$ overestimation) found in May for all years and all platforms except CARIOCA. A similar pattern of annual variability between the Lysbris Seaways record and the SOM-FFN product is seen in all years.

We also compare our SOM-FFN product to both measured $p(CO_2)$ and $p(CO_2)$ calculated from discrete measurements of DIC concentration and TA during the MOSAiC campaign (Fong et al., 2024). Discrete observations from MOSAiC were spatially and temporally aggregated in the same manner as for the quality flag E SOCAT data. The SOM-FFN $p(CO_2)$ product shows the same general pattern as the MOSAiC $p(CO_2)$ observations, with highest values in midwinter and lowest values in the summer (Figure 5). We note that variability in the MOSAiC time series encompasses not only seasonal but also spatial variability (Schulz et al., 2024). Transitions between surface ocean regimes or water masses were often accompanied by sharp changes in biogeochemical properties (Schulz et al., 2024). This is particularly apparent in the latter part of the time series, when the MOSAiC drift relocated for its final leg and crossed between different water masses in the Nansen and Amundsen Basins (Fong et al., 2024). The SOM-FFN $p(CO_2)$ values are lower than the observations. Bottle samples are on average 16 µatm higher than the SOM-FFN product, whereas the underway samples are 7 µatm higher than the SOM-FFN product.

3.1.3. Uncertainties in the $p(CO_2)$ Product

Low data availability acts as a key limitation and leads to uncertainty in $p(CO_2)$ estimates, both on seasonal and regional scales (Gregor et al., 2019; Woolf et al., 2019)—particularly in the High Arctic. As seen in Tables 2 and

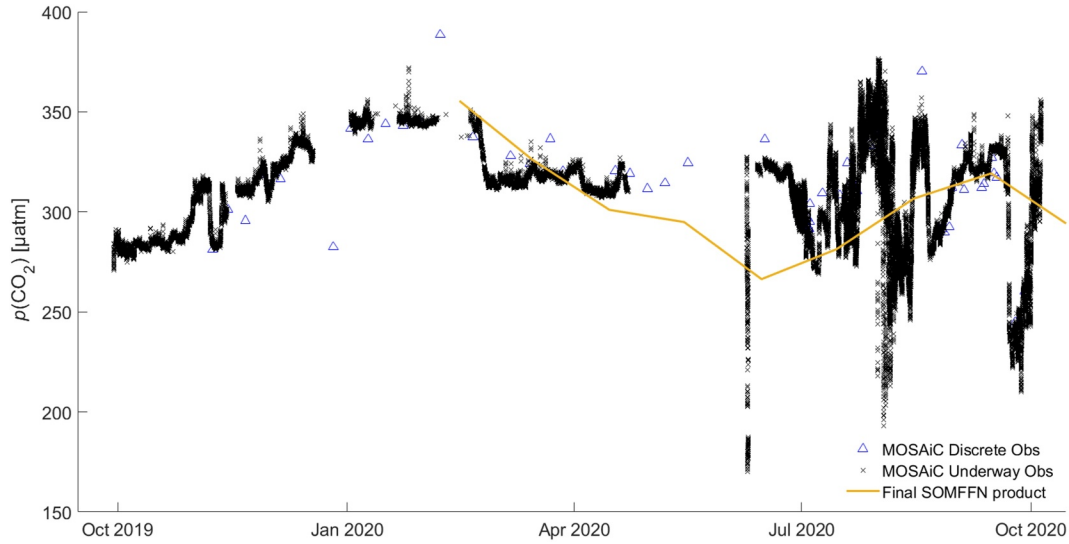

Figure 5. Timeseries of surface ocean $p(CO_2)$ from the MOSAiC drift, both from underway measurements (black), and discrete samples analyzed for Dissolved Inorganic Carbon concentration and Total Alkalinity (blue), as well as from the Self Organising Map–Feed Forward Network product (yellow). Tracks for each timeseries are given in Figure A2.

3, the SOM-FFN product performance is generally poor where fewer SOCAT observations are assimilated by the FFN. Not surprisingly, regions with fewer $p(CO_2)$ observations are subject to greater uncertainty in neural network interpolation methods, highlighting the need for increased and continued sampling (Jersild & Landschützer, 2024). Data availability for environmental drivers, not just $p(CO_2)$, also limits the determination of $p(CO_2)$ values, with missing MLD data preventing the assignment of biogeochemical provinces or subsequent $p(CO_2)$ calculation for 36% of grid cells - mostly in the Russian High Arctic. This has also been noted for the Jersild et al. (2017) SOM-FFN product by Ritschel et al. (2024). Interestingly, SOM-FFN performance outside of areas of lower data availability is also thought to be hindered by lower amounts of input data (Dong, Bakker, & Landschützer, 2024).

Sea ice cover also acts as a significant source of uncertainty for the $p(CO_2)$ product. Firstly, sea ice retrieval errors may impact the demarcation of the ice province. Also, satellite estimates of sea ice cover do not account for the thickness and type of sea ice (and resultant light penetration into the surface ocean below; see Ericson et al., 2023). Backwards extrapolation of relationships between $p(CO_2)$ and sea ice cover by the neural network may be affected by the fact that sea ice type has changed as the Arctic Ocean warms.

As outlined above, we quantify the uncertainty in our $p(CO_2)$ product in terms of measurement, regridding and mapping uncertainties. We can consider the measurement error for $p(CO_2)$ (θ_{obs}) to be that given by the SOCAT cookbook of 2–5 µatm, here we use a value of 5 µatm as a more conservative estimate. We calculate our regridding uncertainty (θ_{grid}) as the mean value of the standard deviation of the SOCAT observations contained within each cell of the SOCAT gridded product, which gives us a value of 2.56 µatm. Finally, for the uncertainty in our SOM-FFN mapping, we take the RMSE between the SOCATv2023 and the SOM-FFN products, giving a θ_{map} of 29.1 µatm, in the range of uncertainty estimates of Yasunaka et al. (2018) and Roobaert et al. (2024). Combining the error sources and using standard error propagation (Equation 1) over the entire Arctic domain, these give us an overall uncertainty of 3.5 µatm for the Arctic Ocean mean $p(CO_2)$ from the SOM-FFN product.

3.1.4. Temporal Trends and Seasonality

Seasonal trends seen in the SOCAT observations are reproduced in the SOM-FFN product, with the decrease in summertime $p(CO_2)$ seen at lower latitudes extrapolated toward the pole. The SOM-FFN product produces a seasonal cycle of $p(CO_2)$ with an amplitude of approximately 50 µatm, roughly half of that seen in SOCAT (Figure 6a). This discrepancy is most evident for latitudes south of 67°N. Earlier products using the SOM-FFN method are known to underestimate the amplitude of seasonal variation in the North Atlantic (Landschützer et al., 2013), thought to be due to the mechanism used to prevent over-training of the neural network.

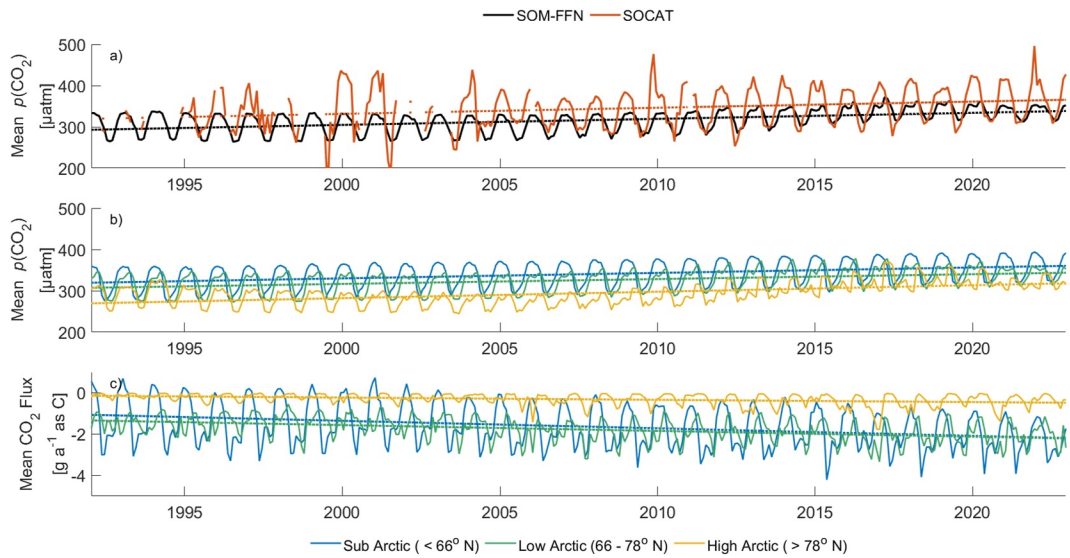

Figure 6. (a) Mean seasonal cycle and temporal trend for the Self Organising Map–Feed Forward Network (SOM-FFN) product (black) and SOCATv2023 (orange) across the entire study area. (b) Mean seasonal cycle and temporal trend from the SOM-FFN product for the three latitude bands. (c) As per (b) but for the CO_2 flux calculated using the Prytherch *K* parameterization with the linear sea ice parameterization and no maximum sea ice threshold (orange/third from the left in Figure 8). We note that the choice here of this flux parameterization is somewhat arbitrary, and find qualitatively similar results for all flux parameterizations tested.

Mean differences between the SOCAT gridded product and the SOM-FFN product are positive throughout most of the year, but become negative during the summer. Observational coverage within SOCAT is biased toward the summer months (Figure A1), particularly at higher latitudes. The differences in the seasonal amplitude and the sign of the mean difference may be an artifact of the amount of data available for interpolation as opposed to a robust difference in seasonal performance. Largest mean (December) and median (April) differences both occur during the ice-covered season when fewer data are available, supporting the fact that this is a function of data availability.

We find an increase in mean surface ocean $p(CO_2)$ between 1991 and 2022, both across the entire Arctic Ocean domain and for our three latitude bands individually (Figure 6). Rates of change of mean $p(CO_2)$ are greatest in the High Arctic, where surface ocean $p(CO_2)$ increases by 18% (a mean increase of 1.6 µatm per year, compared to a mean decrease in atmospheric $p(CO_2)$ in the High Arctic). Surface ocean $p(CO_2)$ for the other two latitude bands increase with increasing atmospheric $p(CO_2)$, but the increase in atmospheric $p(CO_2)$ is greater than that seen for the surface ocean. As mentioned by Yasunaka et al. (2018), temporal changes in $p(CO_2)$ discussed here also include variations due to changes in data coverage over time, with a greater proportion of SOCAT data available to interpolate (both across the domain as a whole, and for each of the three latitude bands) after 2011 (Figure A1). Discontinuities in SOCAT data limit the extraction of similar temporal observational trends to compare against, with observations from the High Arctic not available year-round or prior to 2008. However, the difference between the earliest available and the most recent monthly averages in the SOCAT gridded product shows an increase for all latitude bands, with the largest increase again found in the High Arctic. Such trends are sensitive to the start and endpoints of a time series, and we caution that the rate of change seen both within each latitude band and across our Arctic domain as a whole may not be representative of longer term timescales (Fay & McKinley, 2013). Additionally, with differences in the length of available time series data from SOCAT across the three latitude bands, differences in the rate of increase are likely to occur: data sparsity is known to have an impact on trend estimates of ocean carbon sinks (Hauck et al., 2023).

Increasing mean $p(CO_2)$ values occur in tandem with decreasing sea ice cover. This mirrors previous findings, with the century-long model study of Smedsrud et al. (2022) finding a doubling of ocean CO_2 uptake as a result of sea ice loss in the Barents sea and the central Arctic Ocean. Surface ocean $p(CO_2)$ was also shown to increase coincidentally with decreases in sea ice cover in the neural network approach of Ericson et al. (2023). This is most prominent in the Low Arctic region, where sea ice change is the most acute, with a decrease in the average grid

cell ice cover fraction double that when considering the domain as whole. Decreasing salinity and increasing sea surface temperatures, both most pronounced in this region of greatest sea ice loss, impact the solubility of CO_2 (Weiss, 1974), in turn affecting $p(CO_2)$ values. Relationships between $p(CO_2)$ and the SOM-FFN driving variables differ in the High Arctic from those in the other two latitude bands, likely in part due to ice cover, but also potentially due to ice cover inhibiting the measurement of those variables.

3.2. Air-sea CO_2 Flux

3.2.1. CO_2 Flux Overview

All twelve flux parameterizations tested gave similar spatial patterns of air-sea CO_2 flux, with year-round mean fluxes shown in Figure 7. Most areas act as an ocean carbon sink year-round, but fluxes in the North Pacific and Hudson Bay regions have a seasonally varying sign; the Hudson Bay is a source of CO_2 to the atmosphere in the late summer season and the North Pacific acts as a source from November to March. Other shelf regions are also known to act as seasonal CO_2 sources (e.g., Willcox et al., 2024), but are below the resolution of our $p(CO_2)$ product. The strongest sinks are the Barents Sea, the western Greenland Sea and in the Davis Strait. These areas approximately denote the oceanic margin of the maximum sea ice area. The greatest seasonal variability, from weak sink to strong source, is found in the Bering Strait. Lower fluxes are found in perennially sea ice covered areas. Grid cells in the High Arctic make a considerably smaller contribution to the overall size of the Arctic Ocean carbon sink than those at lower latitudes, although their relative contribution is noticeably greater for non-linear parameterizations of sea ice (10–20%, as opposed to >10% for linear parameterizations; Figure 8). When considering per unit area fluxes, the relative contribution of the different latitude bands varies between parameterizations, with the greatest flux contributions usually from the Low Arctic region.

3.2.2. Parameter Sensitivity of Air-sea CO_2 Flux

Uncertainties in surface ocean $p(CO_2)$ are only one of a number of potential contributors to uncertainty in the final CO_2 fluxes. Previous research on the uncertainty of air-sea CO_2 flux calculations focuses on uncertainties in wind speed and gas transfer as well as uncertainties in both atmospheric and surface ocean $p(CO_2)$ (Jersild & Landschützer, 2024). However, considerations surrounding the parameterization of sea ice in the air sea flux calculation are largely not included within uncertainty synthesis protocols (e.g., Ford et al., 2024; Jersild & Landschützer, 2024). We undertook a sensitivity test looking at three different ways in which uncertainty is introduced into flux estimates in sea ice areas; (a) through the choice of the gas transfer coefficient parameterization (as mentioned in previous studies, although rarely systematically compared for a region of this size), (b) through the scaling of the ocean-atmosphere flux to the sea ice cover and (c) through uncertainties in the retrievals of sea ice cover fraction. Sensitivity testing of the parameterization of air-sea CO_2 flux revealed a difference of 23% or 4.1 Pg in the total size of the entire Arctic Ocean CO_2 sink for the two most extreme cases (Figure 8b) over the course of the 32 years covered by our $p(CO_2)$ product. Of the different air-sea CO_2 flux parameterizations, we found the differences between the linear and non-linear parameterizations of sea ice cover in the flux equation to have the most significant effect on the calculated fluxes and the overall magnitude of the Arctic Ocean carbon sink (Figure 8). A paired samples t-test shows this difference to be statistically significant at the 0.05 level ($p = 0.0084$), with the non-linear parameterization used herein always producing a larger Arctic Ocean CO_2 sink than its linear counterpart. However, we note that newer non-linear parameterizations of the impact of sea concentration on gas transfer velocity suggest that gas transfer velocity (and subsequently CO_2 fluxes) may be suppressed by the presence of sea ice (Loose et al., 2024), and thus decrease, rather than increase, the size of the Arctic Ocean CO_2 sink. This discrepancy highlights that the role of sea ice in regulating CO_2 sink dynamics in the Arctic Ocean remains poorly constrained, with persistent uncertainties surrounding the effect of sea ice on air–sea CO_2 fluxes. Our results showing the scale of the impact of sea ice scaling on the Arctic Ocean carbon sink can be seen to underscore the need for further targeted studies to better understand the complex interplay between sea ice cover, gas transfer processes, and carbon uptake in polar regions.

As the Max 90% Ice parameterization (alternate, less saturated bars in Figure 8) represents a 10% uncertainty in sea ice cover from satellite retrievals (as assumed by Loose et al., 2014) in the flux calculation for both linear and non-linear treatments of sea ice cover, these can be considered as upper estimates rather than true members of the flux ensemble. However, although this results in a small decrease in the average value of the cumulative sink of the Arctic Ocean, the difference is not statistically significant at the 0.05 level. Excluding these cases still results

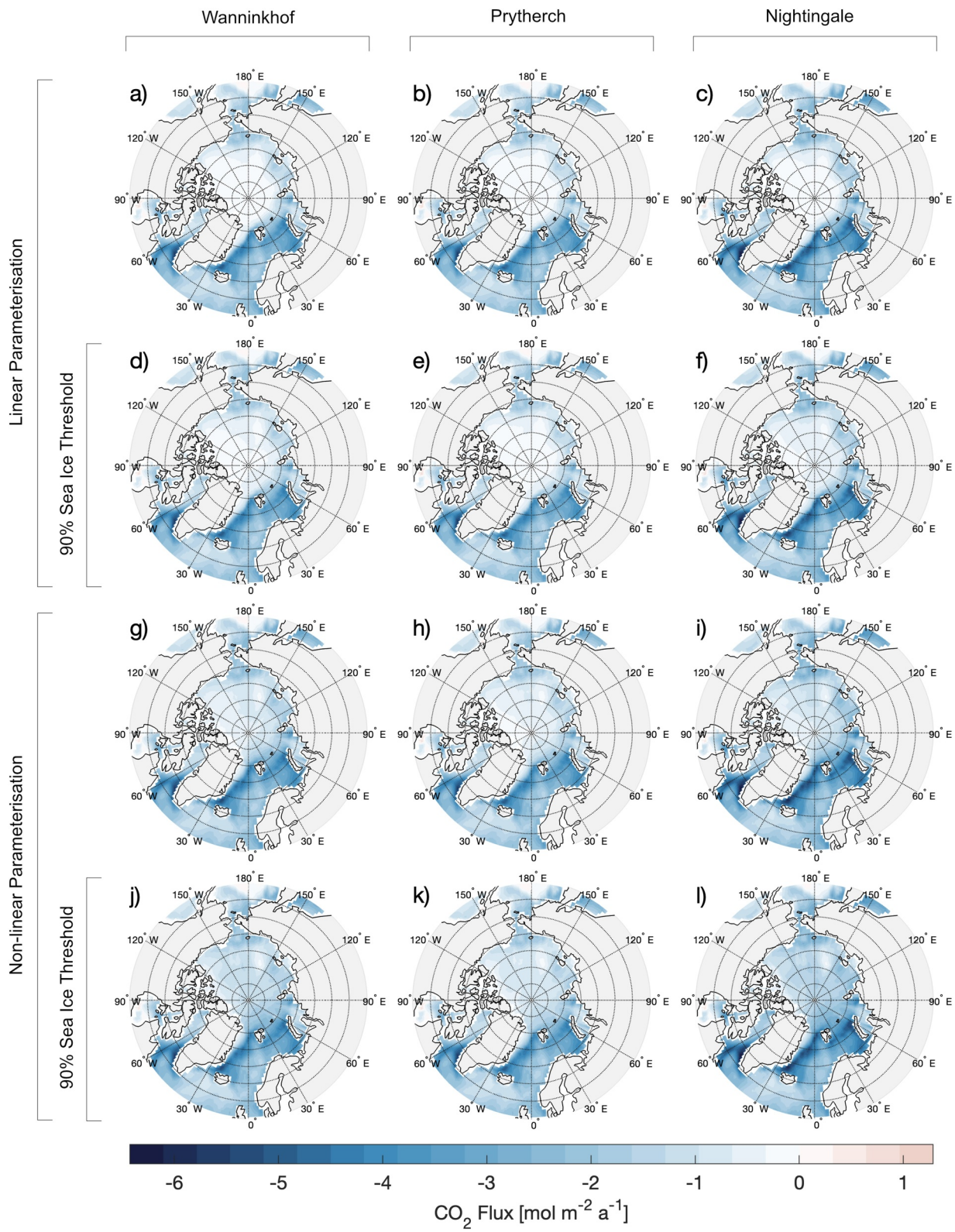

Figure 7. Mean CO_2 flux from all 12 combinations of parameter choices; (a–f) show the linear parameterizations, and (g–l) the non-linear parameterizations; each set shows the parameterization of Wanninkhof (2014, first column; (a, d, g, j)), then Prytherch and Yelland (2021, second column; (b, e, h, k)), then Nightingale et al. (2000, final column; (c, f, i, l)), with the maximum 90% sea ice threshold as the second row in each block. Negative CO_2 fluxes denote ocean uptake (in blue) and positive fluxes denote release (in red) of CO_2 from the ocean to the atmosphere.

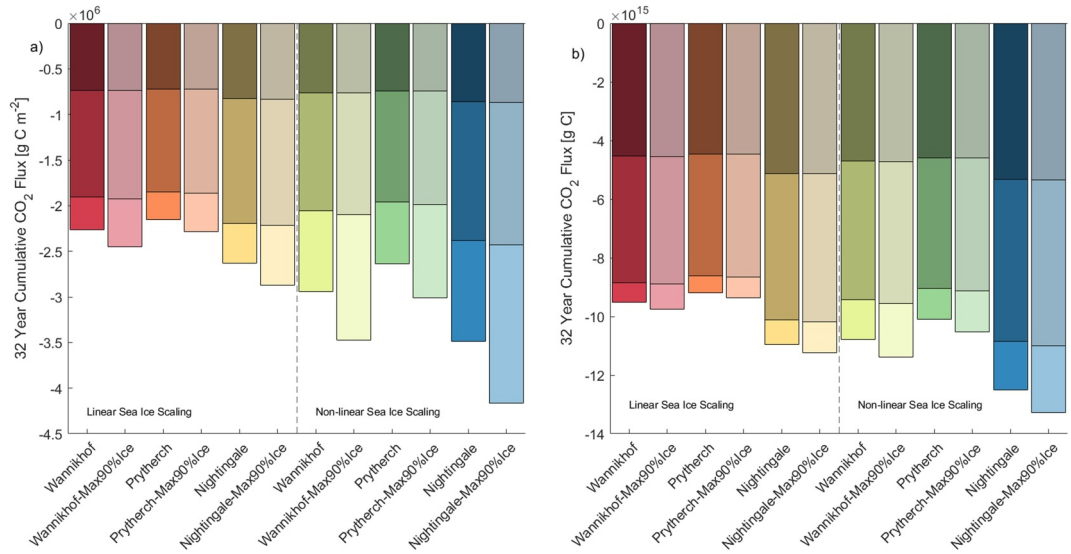

Figure 8. (a) Cumulative CO_2 sink in C equivalents per unit area for the 32 years study period for each of the sea ice parameterizations. Each bar is split into the Sub-Arctic, Low Arctic and High Arctic latitude bands (from top). (b) As for (a) but for the entire model domain rather than per unit area. Note the different scale on the *y*-axes.

in a difference between the most extreme cases of approximately 20% (or 3.3 Pg C) of the total size of the Arctic Ocean CO_2 sink.

Differences in the derived fluxes stem not only from variations in the SOM-FFN product or the sea ice cover, but also from the parameterization of the gas transfer coefficient *k*. Globally, around 30–37% uncertainty in ocean carbon uptake could arise from *k* (Roobaert et al., 2018), with Jersild and Landschützer (2024) expecting this to dominate the uncertainty in polar regions, contributing almost 50% to their calculated total uncertainty. However, we found the choice of *k* to give the lowest contribution to the overall variability: the parameterization option using the *k* value of Prytherch et al. (2017)—applied when the sea ice cover fraction was greater than 0.1, otherwise using the *k* value of Wanninkhof (2014)—gave the lowest absolute CO_2 fluxes, and that of Nightingale et al. (2000) the highest flux values, with the most commonly used parameterization of Wanninkhof (2014) falling in the middle of this range (Figure 8). Differences in the overall size of the Arctic Ocean carbon sink between these gas transfer parameterizations (holding all other choices constant) are always within the 20% uncertainty range quoted in Ford et al. (2024). This is in line with the recent study of Dong, Bakker, Bell, et al. (2024), who suggest that gas transfer parameterizations are not the main reason for disagreement between flux estimates in the Southern Ocean. Our findings indicate that this may be the case for polar oceans more broadly.

We note that other studies investigating the impact of the gas transfer parameterization include multiple wind speed products in their calculation (e.g., Roobaert et al., 2018), which may induce greater uncertainties in the impact of *k*, although the parameterization of the gas transfer coefficient is thought to be more important to the final flux calculated than the wind product used in that equation (Fay et al., 2021). Additionally, wind speed based parameterizations of gas transfer coefficient may become less appropriate at high wind speeds (Wanninkhof, 2014), particularly for low-solubility gases like CO_2. However, with less than 5% of monthly mean wind speeds within our domain over 10 m s^{-1}, the impact of bubble-mediated gas transfer is likely to be small. Wind speed based parameterizations of gas transfer may also be less appropriate in the Arctic sea ice zone due to additional forms of turbulence caused by sea ice (Bigdeli et al., 2018; Loose et al., 2014).

3.2.3. CO_2 Flux Uncertainties

The Arctic chapter of the most recent RECCAP report quantifies the uncertainty in different estimates of the Arctic Ocean carbon sink through the use of the standard deviation of the mean sink (Yasunaka et al., 2023). Applying this method, we find an uncertainty in our 32 year cumulative flux estimate of 1.26 Pg C when considering all 12 of our flux parameterization approaches. If we were to treat the Max 90% sea ice cover

parameterization as an upper bound on potential flux as opposed to a contributor toward the uncertainty estimate, this reduces the standard deviation to 1.19 Pg C over the 32 year period (or 39 Tg C per year). For only the area covered by the RECCAP Arctic definition, we find an uncertainty of 0.72 Pg C compared to their 0.132 Pg C estimate (both over the entire time period of the product; equivalent to 22 Tg C and 4 Tg C a year respectively). We note that their estimate is for a different time period (1985–2017, as opposed to our 1991–2022), and that only 2 of the 8 $p(CO_2)$ products they discuss contribute to their uncertainty estimate.

Additionally, other factors that we have not investigated or explicitly considered may have introduced uncertainty into our flux estimates. All flux parameterizations include temperature and salinity dependencies, with the potential for errors in these to be carried forwards into the calculated CO_2 fluxes; however, (for other gases like dimethyl sulfide at least) this is not thought to be significant (Bock et al., 2021). Ouyang et al. (2022) suggest weighting the gas transfer coefficient by sea ice cover history, not just sea ice cover at that time, as antecedent conditions play an important role in determining current flux - although the application of this is limited by the monthly resolution of our $p(CO_2)$ product and subsequent flux estimates.

3.2.4. Temporal Variability in CO_2 Fluxes

In contrast to the study of Rustogi et al. (2023), we do not see considerable differences in the seasonal variability from the different flux estimates. However, this may not be surprising as all our flux parameterizations use the same underlying $p(CO_2)$ data - and therefore the same seasonality of $p(CO_2)$, whereas their comparison of observations and modeled fluxes will use different $p(CO_2)$ values between observed and modeled fluxes. Differences in the seasonal patterns between parameterizations become more pronounced moving northwards, but even then, the same broad pattern of low spring fluxes and higher uptake in summer and autumn in the High Arctic latitude band are seen for all parameterization options. Differences between parameterizations are more pronounced when fluxes are higher, particularly outside of the Low Arctic.

Unlike Yasunaka et al. (2018), we see a noticeable increase in the size of the Arctic Ocean carbon sink over time for all parameterization choices, with the annual carbon sink increasing by more than 50% over the 32 years of the product (from 0.7 to 1.4 mol m^{-2} a^{-1} to 1.2–2.4 mol m^{-2} a^{-1}, depending on parameterization). Differences between the flux parameterizations are seen when looking at temporal trends for each of the three latitude bands individually, but an increase in the size of the annual carbon sink is seen for each latitude band. In most years, the Sub-Arctic acts as the largest carbon sink, but in some years the Low Arctic is a larger sink, particularly for the non-linear sea ice parameterizations. The carbon sink increases depend on latitude and the chosen flux parameterization. For the non-linear sea ice parameterization, increases are greatest for the Sub-Arctic, whereas for the linear sea ice parameterization, increases are greatest in the High Arctic.

As for $p(CO_2)$, ocean carbon uptake increases as the sea ice area decreases. However, this is not the sole driver of changes in CO_2 flux over time; the highest change of sea ice cover is found in the Low Arctic, but this is not always where the highest change of CO_2 flux is found. Conducting a similar analysis for other climate variables such as second moment wind speed shows no major trends.

3.3. Additional Considerations

In addition to the role of sea ice in controlling surface ocean $p(CO_2)$, and its impact on air-sea fluxes–for example, via release of $p(CO_2)$ to underlying waters or through storage of CO_2 within the sea ice (Richaud et al., 2023), the sea ice surface itself may also be a site of sizable CO_2 fluxes and make its own individual contribution to the Arctic Ocean carbon sink. Fluxes shown herein do not include flux from the ice surface itself, which may be sizable (e.g., Delille et al., 2014; Else et al., 2012; Nomura et al., 2018).

Furthermore, the resolution of the SOM-FFN product may not adequately capture processes occurring in nearshore environments within our study domain, which can influence $p(CO_2)$ dynamics and, consequently, CO_2 flux estimates. For example, processes such as glacial outflow (Duke et al., 2024) and river discharge can affect the CO_2 sink in complex ways. Riverine carbon input may elevate surface water $p(CO_2)$ and thereby reduce CO_2 uptake (e.g., Bertin et al., 2023), while nutrient inputs can stimulate biological activity and enhance CO_2 uptake (Terhaar et al., 2021). The net impact on the CO_2 sink thus reflects a balance between these contrasting processes in nearshore regions, which may ultimately reduce the efficiency of the Arctic Ocean carbon pump, potentially resulting in an increase in future ocean-atmosphere CO_2 fluxes (Oziel et al., 2025). Incorporating relevant

environmental drivers into the SOM-FFN, alongside improved spatial resolution and additional in situ measurements, could help account for these nearshore feedback mechanisms and better constrain $p(CO_2)$ and air–sea CO_2 flux dynamics in this region. This is likely to be disproportionately important in regions such as around Greenland.

Finally, SOCAT classes samples in the upper 10 m of the water column as surface samples, so potential surface ocean stratification effects, with $p(CO_2)$ lower at the air-ocean interface may not be accounted for by the measurements. Dong et al. (2021) suggest that this leads to a 17% underestimation in Arctic Ocean sink strength. Sampling depth is also thought to influence flux calculations due to sea ice processes (Miller et al., 2019), however, their study suggests that sampling within stratified Arctic waters leads to overestimates, not underestimates, of CO_2 flux.

4. Conclusions

We present a new Arctic Ocean $p(CO_2)$ product. The mean difference from SOCAT observations is +1.9 µatm, which is within the measurement uncertainty of those observations. Uncertainty in the surface ocean $p(CO_2)$ values is chiefly due to a lack of input data for the SOM-FFN, and we echo the call for increased observations (Dong, Bakker, & Landschützer, 2024; Hauck et al., 2023; Jersild & Landschützer, 2024; Yasunaka et al., 2023), particularly in ice-covered regions (Kosugi et al., 2017) and in light of rapid changes currently occurring across the Arctic region (Yasunaka et al., 2023). Such observations would not only help to constrain surface ocean $p(CO_2)$ values, but also to better evaluate the suitability of different parameterizations of CO_2 flux. Uncertainties are typically largest, and our evaluation of the $p(CO_2)$ product typically limited, across the Russian Arctic. This is also where most of the missing values in the $p(CO_2)$ product are located.

In line with other studies, we find the Arctic Ocean to act as a sink of CO_2, with the size of the Arctic Ocean carbon sink having increased year-on-year since 1991. However, the absolute size of this carbon sink estimate (9.4–13.3 Pg C over the 32-year study period), and the rate at which this increases, is dependent on the treatment of sea ice. Different parameterizations of sea ice can lead to variability in the size of the Arctic Ocean carbon sink estimates by about 25%, prompting the need to improve our understanding of gas transfer processes in sea ice covered regions.

Appendix A

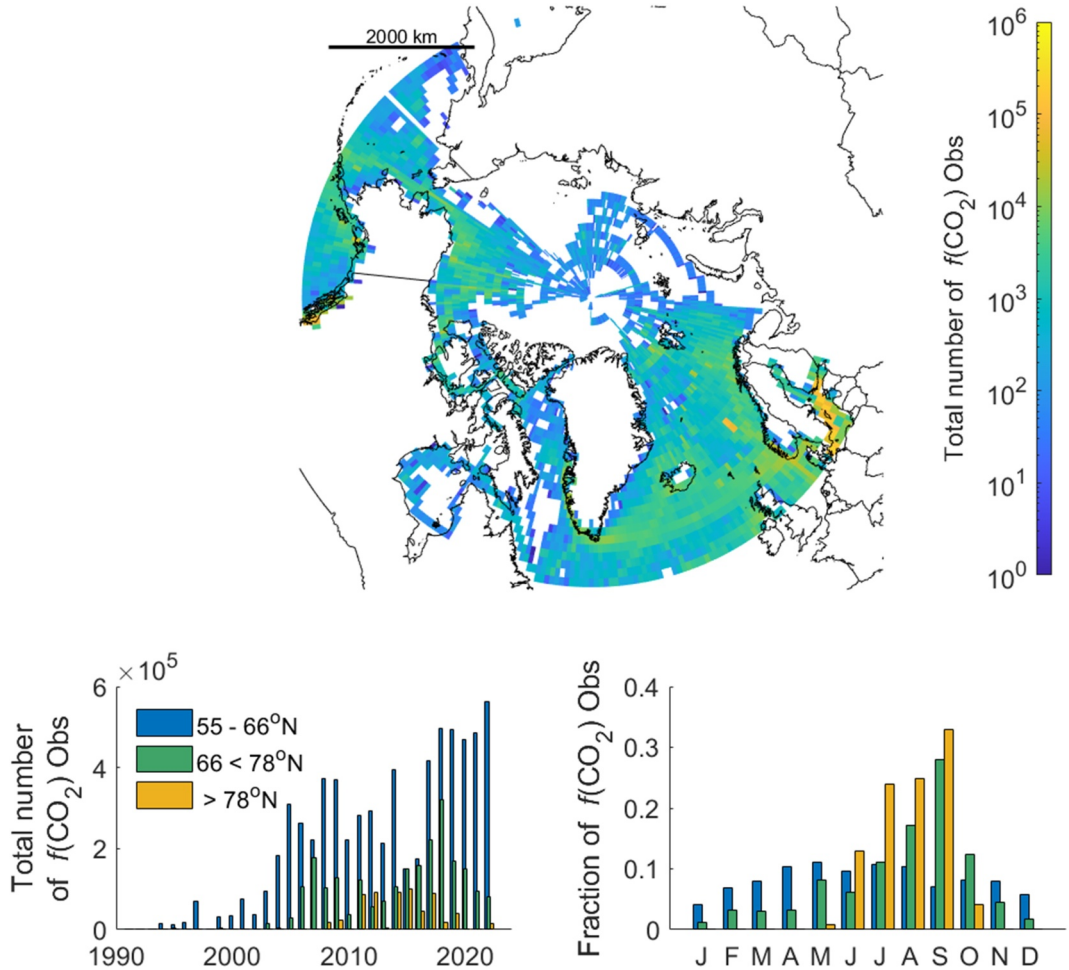

Figure A1. Distribution of surface ocean $f(CO_2)$ (fugacity of CO_2) observations in SOCAT v2023 throughout the spatio-temporal domain of the Self Organising Map–Feed Forward Network product produced herein (plus the Baltic Sea). Bar charts show the distribution in time for the three latitude bands (both annually [left] and seasonally [right]), with the map above showing the spatial distribution. White oceans areas, such as the North coast of Greenland and most of the Siberian Sea, denote where no observations are available.

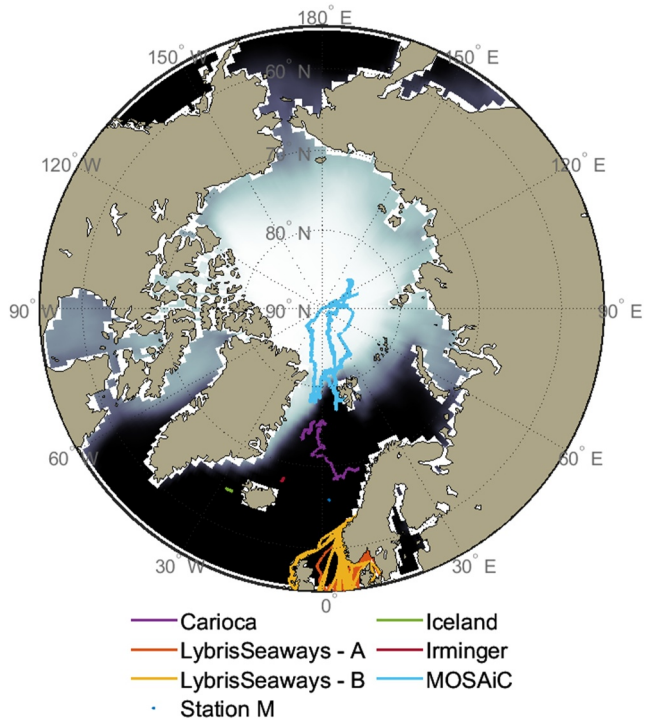

Figure A2. Locations and tracks of all independent timeseries measurements used for evaluation of the surface ocean $p(CO_2)$ or air-sea CO_2 flux product in Section 3.1.2. Ocean shading indicates the 1991–2022 climatological mean sea ice cover, with darker colors representing a lower mean concentration of sea ice.

Data Availability Statement

Forcing data for the SOM-FFN is available as outlined in Table 1. The final $p(CO_2)$ product and all 12 parameterizations from the CO_2 flux sensitivity test are available at Dutch et al. (2025). Plotting and evaluation code available at: https://github.com/V-Dutch/ArcticSOMFFN.

References

Bakker, D. C. E., Alin, S. R., Bates, N., Becker, M., Feely, R. A., Gkritzalis, T., et al. (2023). Surface ocean CO2 atlas database version 2023 (SOCATv2023) (NCEI accession 0278913). *NOAA National Centers for Environmental Information*. https://doi.org/10.25921/r7xa-bt92

Bakker, D. C. E., Alin, S. R., Becker, M., Bittig, H. C., Castaño-Primo, R., Feely, R. A., et al. (2022). *Surface ocean CO_2 atlas database version 2022 (SOCATv2022) (NCEI accession 0253659)*. NOAA National Centers for Environmental Information. https://doi.org/10.25921/1h9f-nb73

Bakker, D. C. E., Pfeil, B., Landa, C. S., Metzl, N., O'Brien, K. M., Olsen, A., et al. (2016). A multi-decade record of high-quality fCO_2 data in version 3 of the surface ocean CO_2 atlas (SOCAT). *Earth System Science Data*, *8*(2), 383–413. https://doi.org/10.5194/essd-8-383-2016

Bates, N. R., & Mathis, J. T. (2009). The Arctic Ocean marine carbon cycle: Evaluation of air-sea CO_2 Exchanges, ocean acidification impacts and potential feedbacks. *Biogeosciences*, *6*(11), 2433–2459. https://doi.org/10.5194/bg-6-2433-2009

Bertin, C., Carroll, D., Menemenlis, D., Dutkiewicz, S., Zhang, H., Matsuoka, A., et al. (2023). Biogeochemical river runoff drives intense coastal Arctic Ocean CO_2 outgassing. *Geophysical Research Letters*, *50*(8), e2022GL102377. https://doi.org/10.1029/2022GL102377

Bigdeli, A., Hara, T., Loose, B., & Nguyen, A. T. (2018). Wave attenuation and gas exchange velocity in marginal sea ice zone. *Journal of Geophysical Research: Oceans*, *123*(3), 2293–2304. https://doi.org/10.1002/2017jc013380

Bock, J., Michou, M., Nabat, P., Abe, M., Mulcahy, J. P., Olivié, D. J. L., et al. (2021). Evaluation of ocean dimethylsulfide concentration and emission in CMIP6 models. *Biogeosciences*, *18*(12), 3823–3860. https://doi.org/10.5194/bg-18-3823-2021

Butterworth, B. J., & Miller, S. D. (2016). Air-sea exchange of carbon dioxide in the Southern Ocean and Antarctic marginal ice zone. *Geophysical Research Letters*, *43*(13), 7223–7230. https://doi.org/10.1002/2016gl069581

Delille, B., Vancoppenolle, M., Geilfus, N.-X., Tilbrook, B., Lannuzel, D., Schoemann, V., et al. (2014). Southern Ocean CO_2 sink: The contribution of the sea ice. *Journal of Geophysical Research: Oceans*, *119*(9), 6340–6355. https://doi.org/10.1002/2014jc009941

Dickson, A. G. (1990). Standard potential of the reaction: $AgCl(s) + iH_2(g) = Ag(s) + HCl(aq)$, and and the standard acidity constant of the ion HSOh in synthetic sea water from 273.15 to 318.15 K. *Journal of Chemical Themodyanmics*, *22*(2), 113–127. https://doi.org/10.1016/0021-9614(90)90074-z

Dlugokencky, E. J., Thoning, K. W., Lang, P. M., & Tans, P. P. (2019). NOAA greenhouse gas reference from atmospheric carbon dioxide dry air mole fractions from the NOAA ESRL carbon cycle cooperative global air sampling network. Retrieved from https://gml.noaa.gov/ccgg/mbl/data.php

Dong, Y., Bakker, D. C. E., Bell, T. G., Yang, M., Landschützer, P., Hauck, J., et al. (2024a). Direct observational evidence of strong CO_2 uptake in the Southern Ocean. *Science Advances*, *10*(30), eadn5781. https://doi.org/10.1126/sciadv.adn5781

Acknowledgments

The Surface Ocean CO_2 Atlas (SOCAT) is an international effort, endorsed by the International Ocean Carbon Coordination Project (IOCCP), the Surface Ocean Lower Atmosphere Study (SOLAS) and the Integrated Marine Biosphere Research (IMBeR) program, to deliver a uniformly quality-controlled surface ocean CO_2 database. The many researchers and funding agencies responsible for the collection of data and quality control are thanked for their contributions to SOCAT. The GLobal interior Ocean biogeochemical DAta Product (GLODAP) is an international effort that would not have been possible without the effort of the many scientists who secured funding, dedicated time to collect data, and shared the data that are included. $p(CO_2)$ data used in this manuscript includes that produced as part of the international Multidisciplinary drifting Observatory for the Study of the Arctic Climate (MOSAiC) with the tag MOSAiC20192020″ and the Project ID AWI_PS122_00. We thank all persons involved in the expedition of the Research Vessel Polarstern during MOSAiC in 2019–2020 as listed in the MOSAiC extended acknowledgment (Nixdorf et al., 2021). This publication has received funding from the European Union's Horizon Europe research and innovation programme under Grant agreement #101056921 (project GreenFeedBack) and from UK Research and Innovation under Grant agreement #10040851. The work reflects only the authors' view; the European Commission and their executive agency are not responsible for any use that may be made of the information this work contains.

Dong, Y., Bakker, D. C. E., & Landschützer, P. (2024b). Accuracy of ocean CO_2 uptake estimates at a risk by a reduction in the data collection. *Geophysical Research Letters*, *51*(9), e2024GL108502. https://doi.org/10.1029/2024GL108502

Dong, Y., Yang, M., Bakker, D. C. E., Liss, P. S., Kitidis, V., Brown, I., et al. (2021). Near-surface stratification due to ice melt biases arctic air-sea CO_2 flux estimates. *Geophysical Research Letters*, *48*(22), e2021GL095266. https://doi.org/10.1029/2021gl095266

Duke, P. J., Hamme, R. C., Ianson, D., Landschützer, P., Ahmed, M. M. M., Swart, N. C., & Covert, P. A. (2023). Estimating marine carbon uptake in the northeast Pacific using a neural network approach. *Biogeosciences*, *20*(18), 3919–3941. https://doi.org/10.5194/bg-20-3919-2023

Duke, P. J., Hamme, R. C., Ianson, D., Landschützer, P., Swart, N. C., & Covert, P. A. (2024). High-resolution neural network demonstrates strong CO_2 source-sink juxtaposition in the coastal zone. *Journal of Geophysical Research: Oceans*, *129*(7), e2024JC021134. https://doi.org/10.1029/2024JC021134

Dutch, V., Bakker, D., Roobaert, A., Landschützer, P., Roden, N., Hoppema, M., & Kaiser, J. (2025). Arctic SOM-FFN product [Dataset–Accompanies article in Global Biogeochemical Cycles]. *Zenodo*. https://doi.org/10.5281/zenodo.15056124

Else, B. G. T., Galley, R. J., Papakyriakou, T. N., Miller, L. A., Mucci, A., & Barber, D. (2012). Sea surface pCO2 cycles and CO2 fluxes at landfast sea ice edges in Amundsen Gulf, Canada. *Journal of Geophysical Research*, *117*(C9), C09010. https://doi.org/10.1029/2012JC007901

Ericson, Y., Fransson, A., Chierici, M., Jones, E. M., Skjelvan, I., Omar, A., et al. (2023). Rapid *f*CO2 rise in the northern Barents Sea and Nansen basin. *Progress in Oceanography*, *217*, 103079. https://doi.org/10.1016/j.pocean.2023.103079

Fay, A. R., Gregor, L., Landschützer, P., McKinley, G. A., Gruber, N., Gehlen, M., et al. (2021). SeaFlux: Harmonization of air–sea CO_2 fluxes from surface CO_2 data products using a standardized approach. *Earth System Science Data*, *13*(10), 4693–4710. https://doi.org/10.5194/essd-13-4693-2021

Fay, A. R., & McKinley, G. A. (2013). Global trends in surface ocean pCO_2 from in situ data. *Global Biogeochemical Cycles*, *27*(2), 541–557. https://doi.org/10.1002/gbc.20051

Fong, A. A., Hoppe, C. J. M., Aberle, N., Ashjian, C. J., Assmy, P., Bai, Y., et al. (2024). Overview of the MOSAiC expedition: Ecosystem. *Elementa: Science of the Anthropocene*, *12*(1), 00135. https://doi.org/10.1525/elementa.2023.00135

Ford, D., Blannin, J., Watts, J., Watson, A., Landschützer, P., Jersild, A., & Shutler, J. (2024). A comprehensive analysis of air-sea CO_2 flux uncertainties constructed from surface ocean data products. Retrieved from https://essopenarchive.org/users/563449/articles/737255-a-comprehensive-analysis-of-air-sea-co2-flux-uncertainties-constructed-from-surface-ocean-data-products?commit=e931c865f4dbfee7286d400b9ba42a66da67c8d9

Friedlingstein, P., O'Sullivan, M., Jones, M. W., Andrew, R. M., Gregor, L., Hauck, J., et al. (2022). Global carbon budget 2022. *Earth System Science Data*, *14*(11), 4811–4900. https://doi.org/10.5194/essd-14-4811-2022

Gerland, S., Barber, D., Meier, W., Mundy, C. J., Holland, M., Kern, S., et al. (2019). Essential gaps and uncertainties in the understanding of the roles and functions of Arctic sea ice. *Environmental Research Letters*, *14*(4), 043002. https://doi.org/10.1088/1748-9326/ab09b3

Gkritzalis, T., Bakker, D. C. E., Lauvset, S. K., & Steinhoff, T. (2024). *SOCAT quality control cookbook–For version 2025 of the surface ocean CO2 atlas*. Tech. Rep. Retrieved from https://socat.info/wp-content/uploads/2025/01/2024_SOCAT_QC_Cookbook_Update.pdf

Gloege, L., Yan, M., Zheng, T., & McKinley, G. A. (2022). Improved quantification of ocean carbon uptake by using machine learning to merge global models and pCO_2 data. *Journal of Advances in Modeling Earth Systems*, *14*(2). https://doi.org/10.1029/2021ms002620

Good, S. A., Martin, M. J., & Rayner, N. A. (2013). EN4: Quality controlled ocean temperature and salinity profiles and monthly objective analyses with uncertainty estimates. *Journal of Geophysical Research: Oceans*, *118*(12), 6704–6716. https://doi.org/10.1002/2013JC009067

Gregor, L., Lebehot, A. D., Kok, S., & Scheel Monteiro, P. M. (2019). A comparative assessment of the uncertainties of global surface ocean CO_2 estimates using a machine-learning ensemble (CSIR-ML6 version 2019a)–Have we hit the wall? *Geoscientific Model Development*, *12*(12), 5113–5136. https://doi.org/10.5194/gmd-12-5113-2019

Gruber, N., Bakker, D. C. E., DeVries, T., Gregor, L., Hauck, J., Landschützer, P., et al. (2023). Trends and variability in the ocean carbon sink. *Nature Reviews Earth and Environment*, *4*(2), 119–134. https://doi.org/10.1038/s43017-022-00381-x

Hauck, J., Nissen, C., Landschutzer, P., Rodenbeck, C., Bushinsky, S., & Olsen, A. (2023). Sparse observations induce large biases in estimates of the global ocean $CO_{(2)}$ sink: An ocean model subsampling experiment. *Philosophical transactions. Series A, Mathematical, physical, and engineering sciences*, *381*(2249), 20220063. https://doi.org/10.1098/rsta.2022.0063

Hersbach, H., Bell, B., Berrisford, P., Horányi, A., Muñoz-Sabater, J., Nicolas, J., et al. (2019). Global reanalysis: Goodbye ERA-Interim, hello ERA5. *ECMWF Newsletter*, *159*, 17–24.

Hood, E. M., Merlivat, L., & Johannessen, T. (1999). Variations of fCO_2 and air-sea flux of CO_2 in the Greenland Sea gyre using high-frequency time series data from the CARIOCA drift bouys. *Journal of Geophysical Research*, *104*(C9), 20571–20583. https://doi.org/10.1029/1999jc900130

Iida, Y., Takatani, Y., Kojima, A., & Ishii, M. (2021). Global trends of ocean CO2 sink and ocean acidification: An observation-based reconstruction of surface ocean inorganic carbon variables. *Journal of Oceanography*, *77*(2), 323–358. https://doi.org/10.1007/s10872-020-00571-5

Jersild, A., & Landschützer, P. (2024). A spatially explicit uncertainty analysis of the air-sea CO_2 flux from observations. *Geophysical Research Letters*, *51*(4), e2023GL106636. https://doi.org/10.1029/2023GL106636

Jersild, A., Landschützer, P., Gruber, N., & Bakker, D. C. E. (2017). *An observation-based global monthly gridded sea surface pCO2 and air-sea CO2 flux product from 1982 onward and its monthly climatology*. NOAA National Centers for Environmental Information.

Jones, S. D., & Henriksen, J. (2018). QuinCe: An online tool for processing and quality control of surface ocean CO_2 measurements. Retrieved from https://imdis.seadatanet.org/content/download/122128/file/IMDIS_2018_submission_45.pdf

Juranek, L. W. (2022). Changing biogeochemistry of the Arctic Ocean: Surface nutrient and CO cycling in a warming, melting north. *Oceanography Society*, *35*(3/4), 144–155. Retrieved from https://www.jstor.org/stable/27182708

Körtzinger, A. (1999). Determination of carbon dioxide partial pressure (pCO_2). In *Methods of seawater analysis* (pp. 149–158).

Kosugi, N., Sasano, D., Ishii, M., Nishino, S., Uchida, H., & Yoshikawa-Inoue, H. (2017). Low pCO_2 under sea-ice melt in the Canada basin of the Western Arctic Ocean. *Biogeosciences*, *14*(24), 5727–5739. https://doi.org/10.5194/bg-14-5727-2017

Landschützer, P., Gruber, N., & Bakker, D. C. E. (2016). Decadal variations and trends of the global ocean carbon sink. *Global Biogeochemical Cycles*, *30*(10), 1396–1417. https://doi.org/10.1002/2015gb005359

Landschützer, P., Gruber, N., Bakker, D. C. E., & Schuster, U. (2014). Recent variability of the global ocean carbon sink. *Global Biogeochemical Cycles*, *28*(9), 927–949. https://doi.org/10.1002/2014gb004853

Landschützer, P., Gruber, N., Bakker, D. C. E., Schuster, U., Nakaoka, S., Payne, M. R., et al. (2013). A neural network-based estimate of the seasonal to inter-annual variability of the Atlantic Ocean carbon sink. *Biogeosciences*, *10*(11), 7793–7815. https://doi.org/10.5194/bg-10-7793-2013

Landschützer, P., Gruber, N., Bakker, D. C. E., Stemmler, I., & Six, K. D. (2018). Strengthening seasonal marine CO_2 variations due to increasing atmospheric CO_2. *Nature Climate Change*, *8*(2), 146–150. https://doi.org/10.1038/s41558-017-0057-x

Landschützer, P., Laruelle, G. G., Roobaert, A., & Regnier, P. (2020). A uniform pCO2 climatology combining open and coastal oceans. *Earth System Science Data*, *12*(4), 2537–2553. https://doi.org/10.5194/essd-12-2537-2020

Lannuzel, D., Tedesco, L., van Leeuwe, M., Campbell, K., Flores, H., Delille, B., et al. (2020). The future of arctic sea-ice biogeochemistry and ice-associated ecosystems. *Nature Climate Change*, *10*(11), 983–992. https://doi.org/10.1038/s41558-020-00940-4

Laruelle, G. G., Landschützer, P., Gruber, N., Tison, J.-L., Delille, B., & Regnier, P. (2017). Global high-resolution monthly CO_2 climatology for the coastal ocean derived from neural network interpolation. *Biogeosciences*, *14*(19), 4545–4561. https://doi.org/10.5194/bg-14-4545-2017

Lauvset, S. K., Key, R. M., Olsen, A., van Heuven, S., Velo, A., Lin, X., et al. (2016). A new global interior ocean mapped climatology: The 1° × 1° GLODAP version 2. *Earth System Science Data*, *8*(2), 325–340. https://doi.org/10.5194/essd-8-325-2016

Lauvset, S. K., Lange, N., Tanhua, T., Bittig, H. C., Olsen, A., Kozyr, A., et al. (2024). The annual update GLODAPv2.2023: The global interior ocean biogeochemical data product. https://doi.org/10.5194/essd-2023-468

Lee, K., Kim, T.-W., Byrne, R. H., Millero, F. J., Feely, R. A., & Liu, Y.-M. (2010). The universal ratio of boron to chlorinity for the north Pacific and north Atlantic oceans. *Geochimica et Cosmochimica Acta*, *74*(6), 1801–1811. https://doi.org/10.1016/j.gca.2009.12.027

Lefèvre, N., & Taylor, A. (2002). Estimating pCO2 from sea surface temperatures in the Atlantic gyres. *Deep Sea Research Part I: Oceanographic Research Papers*, *49*(3), 539–554. https://doi.org/10.1016/S0967-0637(01)00064-4

Lewis, E., & Wallace, D. (1998). CO2SYS: Program developed for CO_2 system calculations. Retrieved from https://www.ncei.noaa.gov/access/ocean-carbon-acidification-data-system/oceans/CO2SYS/co2rprt.html

Loose, B., Fer, I., Ulfsbo, A., Chierici, M., Droste, E. S., Nomura, D., et al. (2024). An analysis of air-sea gas exchange for the entire MOSAiC arctic drift. *Elementa: Science of the Anthropocene*, *12*(1), 128. https://doi.org/10.1525/elementa.2023.00128

Loose, B., McGillis, W. R., Perovich, D., Zappa, C. J., & Schlosser, P. (2014). A parameter model of gas exchange for the seasonal sea ice zone. *Ocean Science*, *10*(1), 17–28. https://doi.org/10.5194/os-10-17-2014

Loose, B., McGillis, W. R., Schlosser, P., Perovich, D., & Takahashi, T. (2009). Effects of freezing, growth, and ice cover on gas transport processes in laboratory seawater experiments. *Geophysical Research Letters*, *36*(5), L05603. https://doi.org/10.1029/2008gl036318

Macovei, V. A., Petersen, W., Brix, H., & Voynova, Y. G. (2021a). Reduced ocean carbon sink in the south and central north sea (2014–2018) revealed from FerryBox observations. *Geophysical Research Letters*, *48*(11), e2021GL092645. https://doi.org/10.1029/2021GL092645

Macovei, V. A., Voynova, Y. G., Gehrung, M., & Petersen, W. (2021b). Ship-of-Opportunity, FerryBox-integrated, membrane-based sensor pCO_2, temperature and salinity measurements in the surface north sea since 2013. *PANGAEA* [dataset publication series]. https://doi.org/10.1594/PANGAEA.930383

Merlivat, L. (2011). *Underway physical oceanography and carbon dioxide measurements during CARIOCA cruise CB_gin96*. PANGAEA. https://doi.org/10.1594/PANGAEA.144801

Miller, L. A., Burgers, T. M., Burt, W. J., Granskog, M. A., & Papakyriakou, T. N. (2019). Air-sea CO_2 flux estimates in stratified arctic coastal waters: How wrong can we be? *Geophysical Research Letters*, *46*(1), 235–243. https://doi.org/10.1029/2018GL080099

Millero, F. J., Pierrot, D., Lee, K., Wanninkhof, R., Feely, R., Sabine, C. L., et al. (2002). Dissociation constants for carbonic acid determined from field measurements. *Deep Sea Research Part I: Oceanographic Research Papers*, *49*(10), 1705–1723. https://doi.org/10.1016/S0967-0637(02)00093-6

National Geophysical Data Center, N. (2006). 2-minute gridded global relief data (ETOPO2). *NOAA National Centers for Environmental Information: National Geophysical Data Center*. https://doi.org/10.7289/V5J1012Q

Nightingale, P. D., Malin, G., Law, C. S., Watson, A. J., Liss, P. S., Liddicoat, M. I., et al. (2000). In situ evaluation of air-sea gas exchange parameterizations using novel conservative and volatile tracers. *Global Biogeochemical Cycles*, *14*(1), 373–387. https://doi.org/10.1029/1999gb900091

Nixdorf, U., Dethloff, K., Rex, M., Shupe, M., Sommerfeld, A., Perovich, D. K., et al. (2021). MOSAiC extended acknowledgement. https://doi.org/10.5281/zenodo.5541624

Nomura, D., Granskog, M. A., Fransson, A., Chierici, M., Silyakova, A., Ohshima, K. I., et al. (2018). CO_2 flux over young and snow-covered arctic pack ice in winter and spring. *Biogeosciences*, *15*(11), 3331–3343. https://doi.org/10.5194/bg-15-3331-2018

Olafsson, J., Olafsdottir, S. R., Benoit-Cattin, A., & Takahashi, T. (2010). The Irminger sea and the Iceland sea time series measurements of sea water carbon and nutrient chemistry 1983–2008. *Earth System Science Data*, *2*(1), 99–104. https://doi.org/10.5194/essd-2-99-2010

Olsen, A., Key, R. M., van Heuven, S., Lauvset, S. K., Velo, A., Lin, X., et al. (2016). The global ocean data analysis project version 2 (GLODAPv2) – An internally consistent data product for the world ocean. *Earth System Science Data*, *8*(2), 297–323. https://doi.org/10.5194/essd-8-297-2016

Ouyang, Z., Li, Y., Qi, D., Zhong, W., Murata, A., Nishino, S., et al. (2022). The changing CO2 sink in the Western Arctic Ocean from 1994 to 2019. *Global Biogeochemical Cycles*, *36*(1), e2021GB007032. https://doi.org/10.1029/2021GB007032

Oziel, L., Gürses, Ä., Torres-Valdés, S., Hoppe, C. J. M., Rost, B., KarakuÅŸ, O., et al. (2025). Climate change and terrigenous inputs decrease the efficiency of the future arctic Ocean's biological carbon pump. *Nature Climate Change*, *15*(2), 171–179. https://doi.org/10.1038/s41558-024-02233-6

Perez, F. F., & Fraga, F. (1987). Association constant of fluoride and hydrogen ions in seawater. *Marine Chemistry*, *21*(2), 161–168. https://doi.org/10.1016/0304-4203(87)90036-3

Popova, E. E., Yool, A., Coward, A. C., Dupont, F., Deal, C., Elliott, S., et al. (2012). What controls primary production in the Arctic Ocean? Results from an intercomparison of five general circulation models with biogeochemistry. *Journal of Geophysical Research*, *117*(C8). https://doi.org/10.1029/2011JC007112

Prytherch, J., Brooks, I. M., Crill, P. M., Thornton, B. F., Salisbury, D. J., Tjernström, M., et al. (2017). Direct determination of the air-sea CO2 gas transfer velocity in arctic sea ice regions. *Geophysical Research Letters*, *44*(8), 3770–3778. https://doi.org/10.1002/2017gl073593

Prytherch, J., & Yelland, M. J. (2021). Wind, convection and fetch dependence of gas transfer velocity in an arctic sea-ice lead determined from eddy covariance CO2 flux measurements. *Global Biogeochemical Cycles*, *35*(2). https://doi.org/10.1029/2020gb006633

Rayner, N. A., Parker, D. E., Horton, E. B., Folland, C. K., Alexander, L. V., Rowell, D. P., et al. (2003). Global analyses of sea surface temperature, sea ice, and night marine air temperature since the late nineteenth century. *Journal of Geophysical Research*, *108*(D14), 4407. https://doi.org/10.1029/2002jd002670

Reynolds, R. W., Smith, T. M., Liu, C., Chelton, D. B., Casey, K. S., & Schlax, M. G. (2007). Daily high-resolution-blended analyses for sea surface temperature. *Journal of Climate*, *20*(22), 5473–5496. https://doi.org/10.1175/2007JCLI1824.1

Richaud, B., Fennel, K., Oliver, E. C. J., DeGrandpre, M. D., Bourgeois, T., Hu, X., & Lu, Y. (2023). Underestimation of Oceanic carbon uptake in the Arctic Ocean: Ice melt as predictor of the sea ice carbon pump. *The Cryosphere*, *17*(7), 2665–2680. https://doi.org/10.5194/tc-17-2665-2023

Ritschel, M., Frajka-Williams, E., & Landschützer, P. (2024). Unlocking the arctic Ocean's carbon cycle: Exploring regional and seasonal changes of surface ocean pCO2 in a warming arctic. Retrieved from https://www.authorea.com/users/82421/articles/1233933-unlocking-the-

arctic-ocean-s-carbon-cycle-exploring-regional-and-seasonal-changes-of-surface-ocean-pco2-in-a-warming-arctic?commit=e9b24b3290b5776bfb8bb34bf92d0da2dad2997c

Rödenbeck, C., Bakker, D. C. E., Gruber, N., Iida, Y., Jacobson, A. R., Jones, S., et al. (2015). Data-based estimates of the ocean carbon sink variability–First results of the surface ocean pCO_2 mapping intercomparison (SOCOM). *Biogeosciences*, *12*(23), 7251–7278. https://doi.org/10.5194/bg-12-7251-2015

Roobaert, A., Laruelle, G. G., Landschützer, P., Gruber, N., Chou, L., & Regnier, P. (2019). The spatiotemporal dynamics of the sources and sinks of CO_2 in the global coastal ocean. *Global Biogeochemical Cycles*, *33*(12), 1693–1714. https://doi.org/10.1029/2019GB006239

Roobaert, A., Laruelle, G. G., Landschützer, P., & Regnier, P. (2018). Uncertainty in the global Oceanic CO_2 uptake induced by wind forcing: Quantification and spatial analysis. *Biogeosciences*, *15*(6), 1701–1720. https://doi.org/10.5194/bg-15-1701-2018

Roobaert, A., Regnier, P., Landschützer, P., & Laruelle, G. (2024). A novel sea surface pCO_2 -product for the global coastal ocean resolving trends over 1982–2020. *Earth System Science Data*, *16*(1), 421–441. https://doi.org/10.5194/essd-16-421-2024

Rustogi, P., Landschützer, P., Brune, S., & Baehr, J. (2023). The impact of seasonality on the annual air-sea carbon flux and its interannual variability. *npj Climate and Atmospheric Science*, *6*(1), 1–8. https://doi.org/10.1038/s41612-023-00378-3

Schmidtko, S., Johnson, G. C., & Lyman, J. M. (2013). Mimoc: A global monthly isopycnal upper-ocean climatology with mixed layers. *Journal of Geophysical Research: Oceans*, *118*(4), 1658–1672. https://doi.org/10.1002/jgrc.20122

Schulz, K., Koenig, Z., Muilwijk, M., Bauch, D., Hoppe, C. J. M., Droste, E. S., et al. (2024). The Eurasian Arctic Ocean along the MOSAiC drift in 2019–2020: An interdisciplinary perspective on physical properties and processes. *Elementa: Science of the Anthropocene*, *12*(1), 00114. https://doi.org/10.1525/elementa.2023.00114

Sharp, J. D., Pierrot, D., Humphreys, M. P., Epitalon, J.-M., Orr, J. C., Lewis, E. R., & Wallace, D. W. (2023). *CO2SYSv3 for MATLAB*. Zenodo. https://doi.org/10.5281/zenodo.7552554

Shupe, M. D., Rex, M., Blomquist, B., Persson, P. O. G., Schmale, J., Uttal, T., et al. (2022). Overview of the MOSAiC expedition: Atmosphere. *Elementa: Science of the Anthropocene*, *10*(1), 00060. https://doi.org/10.1525/elementa.2021.00060

Skjelvan, I., & Lauvset, S. K. (2018). Time series of physical oceanography and carbon dioxide measurements at mooring site station M cruise 589920160522. *PANGAEA*. https://doi.org/10.1594/PANGAEA.891894

Smedsrud, L. H., Muilwijk, M., Brakstad, A., Madonna, E., Lauvset, S. K., Spensberger, C., et al. (2022). Nordic seas heat loss, Atlantic inflow, and arctic sea ice cover over the last century. *Reviews of Geophysics*, *60*(1), e2020RG000725. https://doi.org/10.1029/2020RG000725

Smith, G. C., Allard, R., Babin, M., Bertino, L., Chevallier, M., Corlett, G., et al. (2019). Polar ocean observations: A critical gap in the observing system and its effect on environmental predictions from hours to a season. *Frontiers in Marine Science*, *6*. https://doi.org/10.3389/fmars.2019.00429

Steinhoff, T., Gkritzalis, T., Lauvset, S. K., Jones, S., Schuster, U., Olsen, A., et al. (2019). Constraining the Oceanic uptake and fluxes of greenhouse gases by building an ocean network of certified stations: The ocean component of the integrated carbon observation system, ICOS-oceans. *Frontiers in Marine Science*, *6*. https://doi.org/10.3389/fmars.2019.00544

Sulpis, O., Lauvset, S. K., & Hagens, M. (2020). Current estimates of K_1* and K_2* appear inconsistent with measured CO_2 system parameters in cold Oceanic regions. *Ocean Science*, *16*(4), 847–862. https://doi.org/10.5194/os-16-847-2020

Takahashi, T., Sutherland, S. C., Wanninkhof, R., Sweeney, C., Feely, R. A., Chipman, D. W., et al. (2009). Climatological mean and decadal change in surface ocean pCO2, and net sea–air CO2 flux over the global oceans. *Deep Sea Research Part II: Topical Studies in Oceanography*, *56*(8–10), 554–577. https://doi.org/10.1016/j.dsr2.2008.12.009

Terhaar, J., Lauerwald, R., Regnier, P., Gruber, N., & Bopp, L. (2021). Around one third of current Arctic Ocean primary production sustained by Rivers and coastal erosion. *Nature Communications*, *12*(1), 169. https://doi.org/10.1038/s41467-020-20470-z

Torres-Valdés, S., Rember, R., Heitmann, L., Ludwichowski, K.-U., Ulfsbo, A., Fong, A. A., et al. (2024). Dissolved nutrients data from the PS122 MOSAiC expedition carried out at the AWI nutrient facility. *PANGAEA*. https://doi.org/10.1594/PANGAEA.966217

Torres-Valdés, S., Rember, R., Heitmann, L., Ludwichowski, K.-U., Ulfsbo, A., Fong, A. A., et al. (2024b). Dissolved nutrients data from the PS122 MOSAiC expedition carried out onboard polarstern during legs 1 to 3. *PANGAEA*. https://doi.org/10.1594/PANGAEA.966213

Tremblay, J.-Ã., Anderson, L. G., Matrai, P., Coupel, P., Bélanger, S., Michel, C., & Reigstad, M. (2015). Global and regional drivers of nutrient supply, primary production and CO2 drawdown in the changing Arctic Ocean. *Progress in Oceanography*, *139*, 171–196. https://doi.org/10.1016/j.pocean.2015.08.009

Ulfsbo, A., Chierici, M., Droste, E. S., Nomura, D., Fransson, A., Bakker, D. C. E., et al. (2023). *Dissolved inorganic carbon and total alkalinity of seawater samples during RV POLARSTERN expedition PS122–MOSAiC*. PANGAEA. https://doi.org/10.1594/PANGAEA.954969

Wanninkhof, R. (2014). Relationship between wind speed and gas exchange over the ocean revisited. *Limnology and Oceanography: Methods*, *12*(6), 351–362. https://doi.org/10.4319/lom.2014.12.351

Weiss, R. F. (1974). Carbon dioxide in water and seawater: The solubility of a non-ideal gas. *Marine Chemistry*, *2*(3), 203–215. https://doi.org/10.1016/0304-4203(74)90015-2

Willcox, E., Lemes, M., Juul-Pedersen, T., Sejr, M. K., Holding, J. M., & Rysgaard, S. (2024). The northeast Greenland shelf as a potential late-summer CO_2 source to the atmosphere. *Biogeosciences*, *21*(17), 4037–4050. https://doi.org/10.5194/bg-21-4037-2024

Woolf, D., Shutler, J., Goddijn-Murphy, L., Watson, A., Chapron, B., Nightingale, P., et al. (2019). Key uncertainties in the recent air-sea flux of CO_2. *Global Biogeochemical Cycles*, *33*(12), 1548–1563. https://doi.org/10.1029/2018GB006041

Yasunaka, S., Manizza, M., Terhaar, J., Olsen, A., Yamaguchi, R., Landschützer, P., et al. (2023). An assessment of CO_2 uptake in the Arctic Ocean from 1985 to 2018. *Global Biogeochemical Cycles*, *37*(11), e2023GB007806. https://doi.org/10.1029/2023GB007806

Yasunaka, S., Murata, A., Watanabe, E., Chierici, M., Fransson, A., van Heuven, S., et al. (2016). Mapping of the air–sea CO_2 flux in the Arctic Ocean and its adjacent seas: Basin-wide distribution and seasonal to interannual variability. *Polar Science*, *10*(3), 323–334. https://doi.org/10.1016/j.polar.2016.03.006

Yasunaka, S., Siswanto, E., Olsen, A., Hoppema, M., Watanabe, E., Fransson, A., et al. (2018). Arctic Ocean CO_2 uptake: An improved multiyear estimate of the air–sea CO_2 flux incorporating chlorophyll a concentrations. *Biogeosciences*, *15*(6), 1643–1661. https://doi.org/10.5194/bg-15-1643-2018

Zhong, G., Li, X., Song, J., Wang, F., Qu, B., Wang, Y., et al. (2024). The Southern Ocean carbon sink has been overestimated in the past three decades. *Communications Earth and Environment*, *5*(1), 1–12. https://doi.org/10.1038/s43247-024-01566-6